THE EFFECT OF MONOCYTE CHEMOATTRACTANT PROTEIN-1 CONCENTRATION GRADIENTS ON MONOCYTE MIGRATION IN A THREE-DIMENSIONAL *IN VITRO* VASCULAR TISSUE MODEL

By

NEDA GHOUSIFAM

Bachelor of Science in Chemical Engineering
Sharif University of Technology
Tehran, IRAN
May, 2008

Master of Science in Chemical Engineering
Oklahoma State University
Stillwater, OK
May, 2015

Submitted to the Faculty of the
Graduate College of the
Oklahoma State University
In partial fulfillment of
the requirements for
the Degree of
DOCTOR OF PHILOSOPHY
July, 2015

THE EFFECT OF MONOCYTE CHEMOATTRACTANT PROTEIN-1 CONCENTRATION GRADIENTS ON MONOCYTE MIGRATION IN A THREE-DIMENSIONAL *IN VITRO* VASCULAR TISSUE MODEL

Dissertation Approved:

Dr. Heather Fahlenkamp

Dissertation Adviser

Dr. Sundar V. Madihally

Dr. Josh D. Ramsey

Dr. Sadagopan Krishnan

To My Guardian Angel,

My Mom

Acknowledgements reflect the views of the author and are not endorsed by committee members or Oklahoma State University.

Name: NEDA GHOUSIFAM

Date of Degree: July, 2015

Title of Study: THE EFFECT OF MONOCYTE CHEMOATTRACTANT PROTEIN-1 CONCENTRATION GRADIENTS ON MONOCYTES MIGRATION IN A THREE-DIMENSIONAL *IN VITRO* VASCULAR TISSUE MODEL

Major Field: CHEMICAL ENGINEERING

Abstract:

The initiation of atherosclerosis is marked by the accumulation of lipid substances in the subendothelial layer of major arteries, followed by adhesion and transmigration of monocytes to the extracellular matrix (ECM). Cellular adhesion molecules (CAMs) and chemokines participate in the transmigration of monocytes during the formation of atherosclerotic lesions. Monocyte chemoattractant protein-1 (MCP-1) direct monocytes to the site of inflammation by forming concentration gradients within the ECM. Many studies use two-dimensional (2D) cell culture models to study monocytes migration; however, these models lack the ECM to investigate the formation of MCP-1 gradients within the matrix. In this work, an advanced three-dimensional (3D) *in vitro* vascular tissue model was introduced as a novel tool to study the mechanisms occurring within the ECM that drive monocytes migration. The 3D model consists of human aortic endothelial cells (HAEC) grown on a collagen matrix to better mimic the human artery and surrounding ECM. The main objective of this study was to determine the effect of MCP-1 local concentration gradients within the ECM on monocytes migration. To meet the objective, the 3D tissue model was compared to a 2D model that lacks a matrix and free MCP-1 is diluted in the surrounding medium. Experimental results showed that HAEC on the 2D models had significantly higher CAMs expression than the 3D models after 24 h stimulation. There was no significant difference in MCP-1 expression between models. A greater number of monocytes transmigrated across the endothelium in the 3D tissue model compared to the 2D model. A mathematical model was derived to estimate MCP-1 concentrations within the 3D model at various time points and locations within the matrix. The mathematical model indicates that concentration gradients of both free and bound MCP-1 are formed inside the collagen matrix, and the concentration of bound MCP-1 surpasses the free MCP-1 after 12 h. The results of this research have provided new information regarding the relationship between MCP-1 concentration gradients and monocytes transendothelial migration, due to the effect of haptotactic gradients. The 3D tissue model can also be used to study cellular mechanisms associated with other types of chronic inflammatory diseases.

TABLE OF CONTENTS

Chapter Page

LIST OF TABLES

LIST OF FIGURES

Figure Page

CHAPTER 1

Introduction

1.1 Background and literature review

Cardiovascular disease (CVD) is a major health problem in the world and is one of the leading cause of death in many developed countries. Heart disease and stroke statistics show that more than 200,000 and 830,000 people die from CVD in Europe and USA each year, respectively [1, 2]. The latest National Vital Statistics released by the centers for disease control and prevention (CDC) reports that in United States, heart and cerebrovascular (stroke) diseases are the first and the fifth leading causes of death, respectively [3]. Both diseases can be complications of atherosclerosis.

Atherosclerosis is the primary cause of CVD, including heart attack and stroke [4, 5]. Atherosclerosis is initiated by endothelial dysfunction, inflammation, and extracellular matrix (ECM) remodeling [5, 6]. Plaque formation begins with a subendothelial accumulation of lipid substances, followed by the adhesion of monocytes and lymphocytes to endothelial cells and their subsequent migration across the endothelial layer to the ECM where they differentiate into macrophages and foam cells by consuming lipid substances and interacting with low density lipoprotein [7-13] (Fig. 1). Then, the foam cells start producing inflammatory signals that can cause recruitment of monocytes to the area and the development of an atherosclerosis lesion [13].

As shown in Fig. 2, plaque formation can significantly reduce blood flow in an artery, which may cause a stroke or a heart attack.

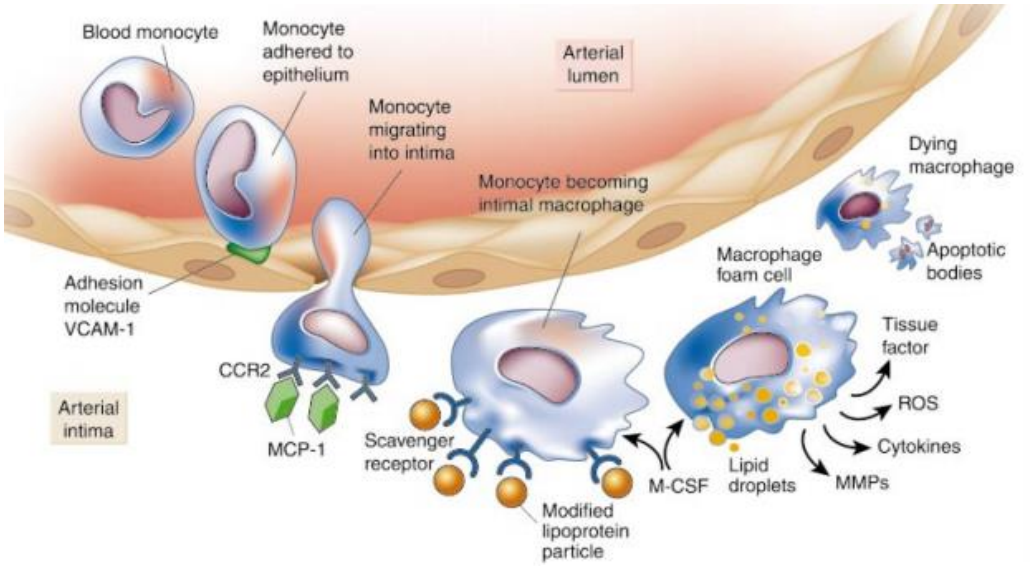

Figure 1. Monocytes adhesion and transmigration cascade through the endothelium [13].

One of the notable events during the initiation of arthrosclerosis is the adhesion and transmigration of leukocytes, such as monocytes and lymphocytes from the blood to the site of inflammation [5, 7, 11, 12, 14-16]. This adhesion and transmigration involves several steps, including slow rolling, adhesion, crawling, paracellular and transcellular migration, and transmigration through the basement membrane. The steps are mediated by many bioactive molecules that are expressed on the endothelium and by the leukocytes [11, 13, 15, 17, 18]. These molecules are called cellular adhesion molecules (CAMs) and chemotactic cytokines (chemokines).

CAMs are proteins expressed on the surface of the cells and are involved in the adhesion of monocytes to the endothelial cell layer [5, 11-13, 15, 18-20]. The CAMs that are relevant to vascular diseases include vascular cell adhesion molecule-1 (VCAM-1), intercellular adhesion molecule-1 (ICAM-1), and platelet endothelial adhesion molecule-1 (PECAM-1).

There is a low to negligible expression of VCAM-1 on unstimulated endothelial cells, and a significant upregulation of VCAM-1 after inflammation. There is an increase of VCAM-1 expression on endothelial cells in an atherosclerosis prone-sites [21, 22]. Pro-inflammatory cytokines, such as interleukin-1β and tumor necrosis factor-α (TNF-α), can stimulate VCAM-1 expression in the endothelium.

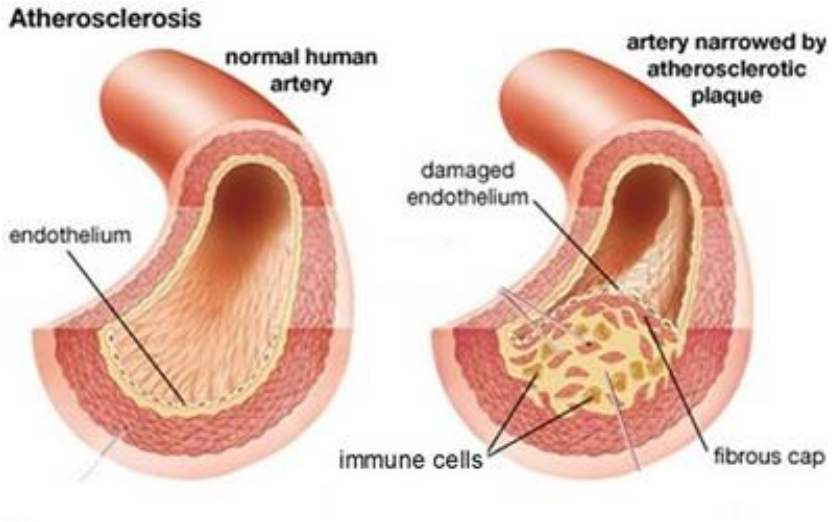

Figure 2. Atherosclerotic plaque formation in an artery.

Picture Source: www.tappmedical.com/atherosclerosis.html

ICAM-1 is expressed on normal endothelium, but the expression is upregulated after stimulation by inflammatory cytokines, such as TNF-α [22-25]. ICAM-1 is expressed highly in the early stages of atherosclerosis and the immunoreactivity of ICAM-1 was shown to be increased significantly at the luminal surface of atherosclerotic lesions [24-29].

PECAM-1 is localized on the cell-cell border of confluent endothelial cell monolayers and to the luminal side of blood vessels [30, 31]. PECAM-1 is key for the transmigration of leukocytes across the endothelium [32] and is not upregulated in response to pro-inflammatory cytokines such as TNF-α and interleukin-1 (IL-1) [33-35].

Chemokines are low molecular weight proteins (8-10 kDa) known to have a pivotal role in immune cell trafficking and activation [17, 36-40]. Chemokines can form concentration gradients as free (fluid phase) or bound (immobilized to the matrix) components [41-48] in the ECM. The free and bound chemokines are responsible for the control of different cellular mechanisms [47, 49], such as migration pattern of dendritic cells and mononuclear leukocytes [46, 48]. The migration of leukocytes from the blood to the tissue site of inflammation is highly dependent on chemotactic gradients [45, 50, 51], such as monocyte chemoattractant protein-1 (MCP-1). MCP-1 (chemotactic toward monocytes and T cells) [52] plays a role in monocytes trafficking across the endothelial layer in an early stages of atherosclerosis [53-55]. The most important feature of MCP-1 is the chemotactic effect on monocytes in both *in vitro* and *in vivo* micro-environments [55, 56]. MCP-1 expression is highly upregulated in an atherosclerotic lesion [54, 57-60], and the formation of an atherosclerotic lesion decreased significantly in the murine models lacking MCP-1 [61, 62].

Previous *in vitro* studies demonstrated that the migration of monocytes is directed by a chemotactic gradient of free MCP-1; however, information about the formation of such a gradient across the endothelial layer is limited [63-67]. It is known that MCP-1 is secreted from endothelial cells in a free form [68], and when the endothelial cells are stimulated, the secretion of MCP-1 was found to be non-polarized [66]. Based on these two findings, it was suggested that *in vivo*, MCP-1 secreted from the apical side of the endothelium was removed continuously by blood flow into the vascular lumen, while the MCP-1 secreted from the basal side diffused into the ECM, thus forming a transendothelial gradient of MCP-1 [66, 68].

Chemokines can bind with the endothelial cell surface and ECM proteins, where the chemokines can be localized and immobilized, forming bound gradients. The binding is believed to be mediated by macromolecule polymers called glycosaminoglycans (GAGs) [44, 47, 69-75]. GAGs on the cell surface and in the ECM can interact with chemokines [44, 47, 69, 70, 72, 75-81] and prevent chemokines from diffusing and being washed away by the blood shear flow [47,

74, 75, 82, 83]. The localized chemokine gradient can direct leukocytes from the blood flow to the subendothelial layer [72].

Handel et al. believe that GAG-chemokine binding interaction is a necessary factor in leukocyte extravasations [74]. The binding between GAG and chemokine is proposed to be ionic, which can be broken by a sodium chloride saline solution [47, 83]. GAGs can also interact with type 1 collagen [84, 85]; therefore, GAG can act as a mediator between MCP-1 and collagen. Further, evidence from a study by Distler et al. has shown that if the binding reaction exists, it is an irreversible reaction [86]. Several studies have investigated chemokine-GAG interaction in the ECM *in vivo* [71-74, 79, 83]; however, the interaction could not be assessed *in vitro* [72, 83, 87] due to the lack of the proper environment to form the haptotactic concentration gradient.

Previous studies have used two-dimensional (2D) experimental systems to investigate the effect of chemokines on monocytes migration [65, 88-90]. Traditional 2D cell culture models may not be suitable predictors of what occurs in more complex three-dimensional (3D) tissue models, like those within the human body [91]. In a 2D model, endothelial cells are grown on a thin, microporous membrane, a chemokine is added to the liquid media below the membrane, monocytes are added to the apical surface of the endothelial cells, and transmigration of the cells across the endothelial cell layer and the microporous membrane is observed [92]. The chemokine is added to both the top and bottom chambers for a chemotactic control [90]. The system is adequate for showing a response of monocytes to a chemokine that has formed an artificial concentration gradient across the endothelial cell layer. However, the diffusive concentration gradient could not be assessed in the 2D models where the free proteins are quickly diluted in the surrounding medium. In the 2D models, endogenous MCP-1 released by the cells to the surrounding liquid media is diluted, quenching the chemoattractant effect. Therefore, a high concentration of MCP-1, relative to *in vivo* conditions, must be added to the bottom chamber to elicit a chemotaxis response [17, 36, 40, 44, 47, 48, 71, 72, 93-96].

A better alternative experimental model is a 3D model consisting of a matrix to mimic the subendothelial ECM. In this study, a collagen matrix is used to represent the ECM and endothelial cells are grown on the surface of the matrix. The major advantage of the 3D model is that the third dimension provides the supplementary space that is significant for the creation of diffusive concentration gradients in the ECM. Apart from this advantage, when focusing on the transmigration of monocytes, this matrix can also provide an appropriate model to investigate the effect of diffusive concentration gradients of MCP-1 on monocytes migration. The 3D model provides an area for monocytes to localize and differentiate after the transendothelial migration. Comparison between the 3D *in vitro* vascular tissue model and the 2D cell culture model is shown in Fig. 3.

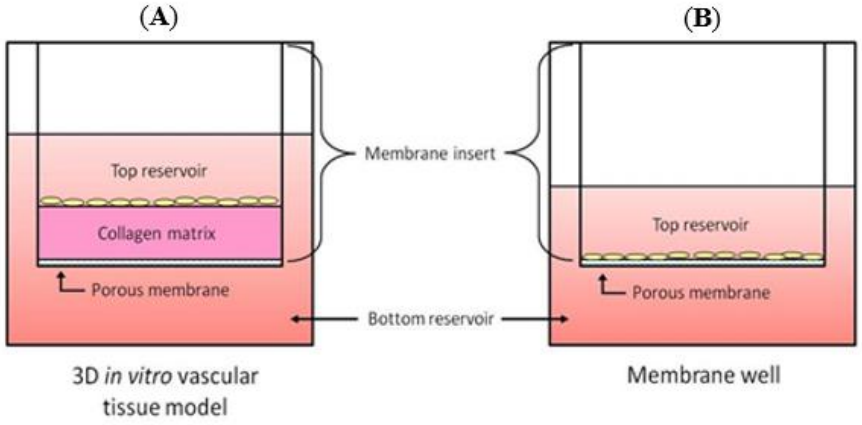

Figure 3. The schematic diagram of **(A)** a 3D *in vitro* vascular tissue model consisting of a collagen matrix would be a better experimental model to mimic the ECM. The 3D tissue model provides the added dimension that is important for the creation of a diffusive concentration gradient formed in the ECM, which is responsible for the control of many cellular mechanisms, and **(B)** a 2D cell culture model where endothelial cells are grown on a thin, microporous membrane, the chemokine is added to the aqueous media below the membrane, monocytes are added to the apical surface of the endothelial cells, and transmigration of the cells across the endothelial cell layer and the microporous membrane is observed.

In this study, an advanced 3D *in vitro* vascular tissue model was introduced as a novel tool to study the MCP-1 concentration gradients and determine the monocytes migration response to the gradients. Overall, the main objective of this work was determining the effect of MCP-1 local concentration on monocytes migration in the 3D tissue model and comparing the outcomes to the 2D model results. We hypothesized that the MCP-1 concentration gradient within the ECM of the 3D tissue model drives a different cellular response than that in the 2D model.

1.2 Project objective and specific aims

The main objective of this study was to determine the effect of MCP-1 local concentration gradients on monocytes migration by using a 3D tissue model and comparing the outcomes to a 2D model. We hypothesized that the MCP-1 concentration gradient within the ECM of the 3D tissue model will drive a different cellular response than that in the 2D model. To meet the objective of the proposed work, the following specific aims were completed:

1) Compare the expression of selected CAMs and MCP-1 on the surface of endothelial cells in the 3D *in vitro* vascular tissue model to those in the 2D cell culture models during inflammation. CAMs are critical participants in the adhesion of monocytes into the atherosclerosis lesion. Therefore, measuring the expression of CAMs and MCP-1 on the surface of the endothelial cells within the 3D and 2D models is necessary to later facilitate understanding the monocytes migration process.

2) Compare the release of MCP-1 from cells within the 3D *in vitro* vascular tissue model to those in the 2D cell culture models during inflammation. MCP-1 released from the endothelial cell layer can diffuse into the ECM and form concentration gradients that can have an effect on monocytes migration. Hence, this step quantifies the concentration of released MCP-1 within the 3D and 2D models. The amount of MCP-1 released from the endothelial cells in the 3D tissue model was used to develop a mathematical model that could be used to determine the

MCP-1 concentration gradients within the matrix of the 3D tissue model at various time points and locations.

3) Determine the effect of MCP-1 release on monocytes transmigration during inflammation. In order to investigate the potential differences in monocytes migration due to the concentration gradient associated with the 3D *in vitro* vascular tissue model, monocytes adhesion and transmigration across the endothelium was compared to the 2D cell culture model.

Overall, the outcome from this project will provide 1) new information regarding the effect of MCP-1 local concentration gradients on monocytes transendothelial migration during an inflammatory response, and 2) a comparison of how cells generally behave within a 3D tissue model versus a 2D model. The results can be used to develop therapeutic strategies for chronic inflammatory diseases that can then be tested in the 3D tissue model.

1.3 Project significance

This project is significant because it provides new information about the early stages of atherosclerosis and a novel 3D tissue model that can potentially be used to test therapeutics for atherosclerosis. The 3D tissue model was used to predict local concentration gradients of MCP-1 within the ECM and to determine the effect on monocytes migration, associated with the early stages of atherosclerosis. Previous work has shown that MCP-1 can bind to ECM proteins and form a bound concentration gradient within the ECM. Therefore, the model was used to determine the contribution of both free and bound MCP-1 gradients within the ECM. The 3D tissue model was compared to existing 2D models in order to show the influence of the ECM making up the third dimension on cell behavior. The expression of CAMs on the endothelial cells, MCP-1 release, MCP-1 diffusive gradients, and monocytes migration were compared between the 3D and 2D models. Findings from comparing the two systems contribute to a better

understanding of how cells behave in 2D versus 3D models and the development of an improved experimental system.

1.4 Preliminary studies

Monocytes are a type of blood immune cells known to transmigrate across the endothelial cell layer continuously. The end state of the monocytes after extravasations is highly dependent on many factors, including the tissue involved in the process, the kind of stimulus (hyperglycemia and TNF-α), and the chemokine concentration gradient in the tissue. These factors were investigated in preliminary studies and the relevant results were used to define the current work. The first subsection describes initial studies of using a 3D tissue model to investigate the effect of glucose concentration on endothelial cell behavior [97]. Studies were performed to examine changes in cell function associated with inflammation by measuring the expression of key cell surface proteins and leukocyte migration across the endothelium. The remaining subsections describe preliminary work that shows MCP-1 concentration profile formation in the ECM [98] and the effect on monocytes migration. The binding reaction between MCP-1 and the collagen matrix is also investigated.

1.4.1 The effect of hyperglycemia on endothelial cells behavior and monocytes migration and differentiation in a 3D tissue model

Hyperglycemia is one of the common complications associated with diabetes and is an inflammatory signal that enhances leukocyte migration across the endothelium. To date, studies to characterize monocytes migration and differentiation in response to hyperglycemia have not been conducted. An initial study conducted by Shukla et al. [97] investigated the use of a 3D tissue model to investigate the effect of hyperglycemia on endothelial cell dysfunction and on immune cell trafficking and differentiation [97].

Briefly, Human Umbilical Vein Endothelial Cells (HUVEC) were seeded on top of the collagen matrix within microwell plates. The cells were incubated with 15 and 30 mM glucose concentration in the culture media for nine hours periods to represent hyperglycemic conditions. The addition of 5.6 mM glucose (normoglycemia) and 10 ng/ml TNF-α (inflammation) were used as negative and positive controls, respectively. The studies were performed to examine changes in cell function by measuring expression of key cell surface markers associated with inflammation and leukocyte migration across the endothelium. The cell surface expression of PECAM-1, VCAM-1, ICAM-1, and E-selectin was detected on the cells surface. Expression of VCAM-1 was only detected for the 30 mM and positive control samples (TNF-α) but not for the 5.6 mM and 15 mM samples, indicating that this adhesion molecule plays a possible role in leukocyte recruitment for the tissue model. PECAM-1 was detected for all of the samples tested with no significant difference among the samples. E-selectin was not detected for any of the samples tested in comparison with the appropriate isotype control. ICAM-1 was only detected for the positive control sample (TNF-α). The supernatants from the samples were also collected and soluble VCAM-1 was measured by ELISA which showed a detectable level of sVCAM-1 within the culture supernatant for a positive control.

Further preliminary studies were performed with the 3D model to investigate the effect of glucose concentration on leukocyte migration and differentiation [97]. After incubation with high concentrations of glucose, the medium was removed and samples were washed, and seeded with PBMCs. Leukocyte migration and cell differentiation characteristics were determined after sample collection. It was shown that the total number of cells in the tissue was increasing after 2 and 48 h incubation as the glucose concentration increased. However, there was no significant change in the reverse-transmigrated cells after 48 h. Furthermore, no significant migration of B-cells (CD19+) or natural killer cells (CD56+) cells across the endothelium into the subendothelium space was observed. However, a significant migration of monocytes (CD14+) and T-cells (CD3+) cells were observed across the endothelial cell layer. There was also a 32%

increase in the number of cells in the subendothelial matrix that were differentiated into macrophages in response to an increase in glucose concentration which showed that the high glucose concentration altered the proportion of monocyte-derived dendritic cells to monocyte-derived macrophages.

This preliminary work demonstrated the feasibility of applying a 3D model to study cell behavior which included: 1) growing a confluent endothelium on a matrix to represent the ECM, 2) endothelial cell response to different stimulus, such as hyperglycemia and TNF-α, and 3) transmigrating and differentiation of monocytes in the subendothelial space as the local concentration of glucose in the model is increased.

1.4.2 MCP-1 and collagen binding reaction test

To focus on the diffusive and kinetic behavior of MCP-1 in the collagen matrix, a simplified collagen matrix without endothelial cells was used by Leemasawatdigul et al. [98]. Complete medium with a known concentration of MCP-1 was added to the top of the simplified collagen model and incubated at standard conditions for a set time period to allow MCP-1 to diffuse from the top reservoir through the collagen matrix and to the bottom chamber. At the end of the incubation time point, the amount of MCP-1 in the solutions from the top and bottom chambers were analyzed by the enzyme-linked immunosorbent assay (ELISA), and the total concentration of MCP-1 in the collagen matrix was calculated. Results showed that the concentration in the collagen matrix was higher than the concentration of MCP-1 which was added initially to the top reservoir. At equilibrium, the concentration of MCP-1 in the top chamber, collagen, and bottom chamber should be equal. A higher concentration than the initial indicated that a reaction is present that consumes MCP-1 or transforms MCP-1 from the free form. This result indicated that MCP-1 can bind with the collagen and forms a bound (nonsoluble) form of MCP-1.

This finding is significant because it was shown that MCP-1 can bind to ECM components and produce bound complexes across the matrix. The finding was used in the current project of a more complex system that includes endothelial cells grown on the collagen matrix that secret MCP-1. Released MCP-1 from the cells can diffuse through the matrix and bind with collagen.

1.4.3 Derivation of a mathematical model to describe the transport of MCP-1 through a 3D collagen matrix without cells

Diffusion of MCP-1 in the 3D simplified collagen matrix without endothelial cells was modeled as unsteady-state diffusion in one dimension by Leemasawatdigul et al. [98]. The equation of continuity, along with experimental data, was used to derive a mathematical model that can be used to estimate MCP-1 concentration gradients within the 3D model. The Crank-Nicolson numerical method was selected to solve the partial differential equation with initial and boundary conditions. The values for the model constants, K_b (reaction rate constant) and $D_{M/C}$ (diffusive coefficient of MCP-1 through the collagen matrix) were determined as 0.858 h^{-1} and 0.108 $mm^2\ h^{-1}$, respectively, by fitting the mathematical model to selected experimental data. The concentration profiles of free and bound MCP-1 in the collagen matrix at set time points were calculated by using the mathematical model. Results of the mathematical model show that the concentration gradient of free MCP-1 decreases overtime, whereas the gradient of bound MCP-1 increases. This finding suggests that apart from the gradient of free MCP-1, the gradient of bound MCP-1 is another potent factor that may mediate monocytes transendothelial migration. For the current project, the mathematical model was modified and solved for a more complex system that includes a source term to account for MCP-1 production from the endothelial cell layer above the collagen matrix. The modified mathematical model provides a way to study the formation of the gradient of MCP-1 that is secreted from endothelial cells and the effect of the gradient on monocytes migration involved in the early stages of atherosclerosis.

1.4.4 The haptotactic effect of MCP-1 on monocytes migration

Previous studies demonstrated the existence of the binding reaction between MCP-1 and collagen. Additional studies were performed to measure the haptotactic effect of MCP-1, from the bound MCP-1 within the 3D model. Briefly, 50 ng/ml of MCP-1 was added to the top of the collagen matrix. After 24 h incubation period, the top and bottom solutions were collected, and the collagen matrix was washed three times to ensure that all free MCP-1 was removed from the collagen matrix. The concentration of MCP-1 in the top and bottom solutions, along with the three wash solutions was measured by the ELISA. A total mass balance for the closed system was used to calculate the concentration of MCP-1 in the collagen matrix. Results showed that 40% of the MCP-1 that was originally added to the top of the collagen matrix and incubated for 24 h, remained in the collagen matrix. The final concentration of MCP-1 in the collagen matrix after three successive washes was four times higher than the initial concentration.

Further, the migration of monocytes into the collagen matrix with bound MCP-1 (as described above) was compared with migration of monocytes into collagen that was not treated with MCP-1. The results revealed that the total number of monocytes that migrate into the collagen matrix with MCP-1 increased significantly compared to when the collagen was not treated. The results from this study demonstrated that in addition to the gradient of free MCP-1, a gradient of bound MCP-1 (haptotactic gradient) was also formed in the collagen matrix as a result of the binding reaction, which can induce monocytes trafficking in to the collagen matrix of the 3D model. The effect of the free/bound gradient of MCP-1 released from endothelium on monocytes transmigration was investigated in the current project.

CHAPTER 2

Effects of Local Concentration Gradients of Monocyte Chemoattractant Protein-1 on Monocytes Adhesion and Transendothelial Migration in an *In Vitro* Three-Dimensional Tissue Model

2.1 Introduction

Atherosclerosis, the primary cause of cardiovascular disease (CVD) [4, 5], is an inflammatory disease and is characterized by endothelial dysfunction, inflammation, and extracellular matrix (ECM) remodeling [5, 6]. Atherosclerotic plaque formation begins with accumulation of lipids in the subendothelial layer of major arteries, followed by the adhesion of monocytes and lymphocytes to the endothelium, and the subsequent recruitment of these cells across the endothelium and into the ECM [7-12]. Plaque formation can significantly reduce blood flow in an artery, which may cause a stroke or heart attack. The adhesion and transmigration of leukocytes across the endothelium include their rolling, adhesion, and crawling which is followed by their paracellular and transcellular migration through the basement membrane [67, 99]. Generation of inflammatory signals regulates cellular movement and differentiation of leukocytes from the circulation into the injured tissue in order to aid in wound healing processes. Cellular adhesion molecules (CAMs) and inflammatory chemotactic cytokines (chemokines) are responsible for the recruitment of leukocytes to the site of inflammation.

Many cardiovascular diseases, such as atherosclerosis, induce inflammation and result in the over-recruitment of leukocytes [10, 38, 40, 52, 54]. Past studies show that specific chemokine profiles dictate the migration of leukocytes to the site of inflamed tissue [40, 66].

CAMs are proteins expressed on the surface of the cells and are involved in the adhesion of monocytes to the endothelial cell layer [5, 11-13, 15, 18-20]. The CAMs that are relevant to vascular diseases include vascular cell adhesion molecule-1 (VCAM-1), intercellular adhesion molecule-1 (ICAM-1), and platelet endothelial adhesion molecule-1 (PECAM-1). Chemokines are low molecular weight proteins (8-10 kDa) known to have a pivotal role in immune cells trafficking and activation [17, 36-40]. The migration of leukocytes from the blood to the tissue site of inflammation is dependent on chemotactic gradients [45, 50, 51], such as monocyte chemoattractant protein-1 (MCP-1). MCP-1 (chemotactic toward monocytes and T cells) [52] plays a role in monocytes trafficking across the endothelial layer in early stages of atherosclerosis [53-55]. Furthermore, it has been shown that MCP-1 expression is highly upregulated in an atherosclerotic lesion [54, 57-60], and the formation of the lesion decreased significantly in the murine models lacking MCP-1 [61, 62].

Previous *in vitro* studies illustrate that the transendothelial migration of monocytes depends on the concentration gradient of free MCP-1 across the endothelial layer [63-67, 88-90]. The highest concentration of MCP-1 is at the source of atherosclerotic inflammation in the arterial walls [38]. Further, MCP-1 is shown to be secreted from the endothelial cell layer in a free form [68], and when the endothelial cells are stimulated, the secretion of MCP-1 was found to be non-polarized [66]. Based on these two findings, it was suggested that *in vivo*, MCP-1 secreted in the luminal side could be prevented by the blood flow into the vascular lumen, while the concentration gradient of MCP-1 is formed within the ECM via the diffusion of MCP-1 released from the basal side of the endothelial cell layer into the subendothelial ECM [68]. Therefore, formation of the MCP-1 concentration gradient is driving monocytes migration into the ECM. However, in response to an inflammatory stimuli, influx of monocytes to the site of

injury increases dramatically, and an atherosclerosis lesion may develop, which is the basis of pathology in atherosclerosis. Presently, profiling the development of MCP-1 gradients in the ECM is still lacking; due to there are no available techniques that can be used to quantify such gradients.

Two-dimensional (2D) cell culture models have been used to investigate the effect of the concentration gradient of free MCP-1 on monocytes migration [88-90]. The model is adequate for showing a response of monocytes to a chemokine that has formed a concentration gradient across a membrane with/without the endothelial cell layer; however, the 2D model cannot be used to examine chemokine concentration gradients that are present within the tissue *in vivo* [17, 36, 40, 44, 47, 48, 71, 72, 93-96]. In the 2D experimental model, endogenous MCP-1 released by the cells to the surrounding liquid media is diluted, quenching the chemoattractant effect. Hence, the model has been used to investigate monocytes migration in response to free exogenous chemokines. Using 2D models for chemotaxis studies can be too simplistic and overlook what occurs *in vivo* due to the lack of a third dimension [91] and they may not be suitable for predicting what occurs in a complex three-dimensional (3D) model, like those within the human body [91]. A better alternative experimental model is a 3D model consisting of a collagen matrix to mimic the subendothelial ECM as proposed here. In this study, an advanced 3D *in vitro* vascular tissue model (defined as 3D tissue model throughout the text) was introduced as a tool to study the underlying mechanisms occurring within the ECM in atherosclerosis. The major advantage of the 3D tissue model is that the third dimension provides the supplementary space that is significant for the creation of MCP-1 diffusive concentration gradients in the ECM, which is responsible for the control of many cellular mechanisms.

In the previous study, we have demonstrated the formation of the MCP-1 diffusive concentration gradient in a simplified, cell-free 3D matrix and have derived a mathematical model to describe the such a gradient [98]. In this study, human aortic endothelial cells (HAEC) are added to the model to form an endothelium on the surface of a collagen matrix used to

represent the ECM. MCP-1 released from the endothelial cell layer can diffuse into the ECM and form localized concentration gradients which can influence the monocytes migration. The goal of the current study is to investigate the effect of MCP-1 local concentration gradients on monocytes migration in the 3D tissue model and compare the outcomes to the existing 2D model results. We hypothesize that the MCP-1 concentration gradient within the ECM of the 3D tissue model would drive a different monocytes migration response than in the 2D model based on the difference in the nature of existing concentration gradients in the 3D and 2D microenvironments.

HAEC growth characteristics (i.e., viability, trans-endothelial electric resistance, and morphology), the kinetic and magnitude expression of the CAMs (VCAM-1, ICAM-1, PECAM-1) and MCP-1, and transport properties (MCP-1 release profile) is also studied between the 2D and the 3D models. The experiments are performed under quiescent conditions and when models are immunologically activated with tumor necrosis factor-α (TNF-α). TNF-α was used to mimic inflammation that occurs in the early stages of atherosclerosis. Differences between two models characteristics, such as endothelium cell behavior, MCP-1 diffusive concentration gradients, and their effect on monocytes transendothelial migration will help us to have a better understanding of underlying mechanisms during an inflammatory response in early stages of atherosclerosis. The results of this research will lead to the development of an improved *in vitro* model to test therapeutic strategies associated with inflammatory diseases.

2.2 Methods

2.2.1 Cell culture

Human aortic endothelial cells (HAEC) and endothelial cell complete medium were purchased from PromoCell, Heidelberg, Germany. HAEC were cultured in 75 cm^2 flasks and incubated at standard conditions (37 °C and humidified atmosphere of 5% CO_2) and used at 90% confluence.

2.2.2 Preparation of the 3D *in vitro* vascular tissue model

Costar (Corning life sciences, Cambridge, MA) and ThinCert Transwells® (Greiner Bio-one, Frickenhausen, Germany) with 8.0 μm permeable membranes were used to create the 3D tissue model in 24 and 12-well inserts, respectively. The inserts provide easy access to the free factors released in the apical and basal compartments of the endothelial layer in the 3D tissue model for taking measurements that makes them more advantageous than other models. Collagen type I solution of the 3D tissue model was prepared using previously described protocols [97, 98] and added to the top of the membrane (78 and 266 μl per well for 24 and 12-well inserts, respectively). Plates were incubated at standard conditions to form a gel. Complete medium was added to the upper and lower chambers and incubated overnight to equilibrate the collagen matrices. The next day, the gel was coated with fibronectin (Biomedical Technologies, Stoughton, MA) and seeded with HAEC ($7.5*10^4$ cells/cm^2). The cells were incubated and used for experiments at one day after reaching confluency and forming an endothelium by visual observation (Fig. 4).

To construct the collagen-coated and 2D models, membranes (8.0 μm pore size) were coated with collagen (15 μl per well for 24-well format inserts) and fibronectin; or fibronectin only, respectively, seeded with HAEC as stated above, and used at one day post-confluence.

Table 1. 24-well format membrane insert characteristics

Membrane Material	Growth Area	Membrane Thickness	Pore Density	Pore Size	Optical Quality
Polycarbonate	0.33 cm^2	10.0 μm	$1*10^5$ pores/cm^2	8.0 μm	Translucent

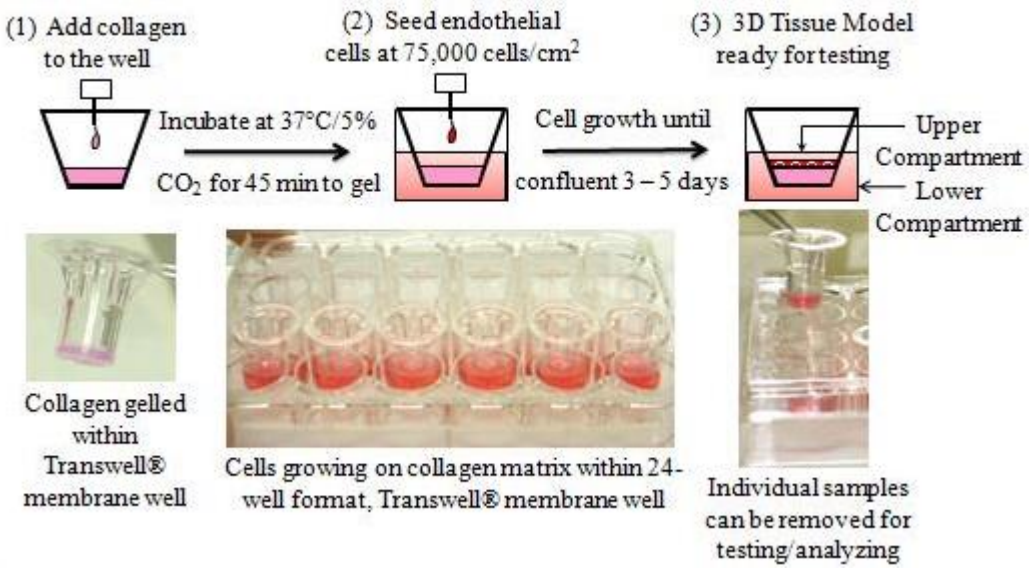

Figure 4. The steps to construct the 3D tissue model within the Transwell permeable supports. Briefly, a 57.1 vol % bovine collagen type I solution was prepared and added to the top of the membrane and incubated at 37 °C and 5% CO_2 to form a gel. Complete endothelial cell growth medium was added to the top and bottom chamber and incubated overnight at standard conditions to equilibrate the collagen matrices. The next day, the matrices were seeded with HAEC ($7.5*10^4$ cells/cm^2) and cells confluency was monitored everyday by visual observation. Samples were used for experiments at post-day reaching confluency.

2.2.3 HAEC viability and trans-endothelial electric resistance

Viability and unit area resistance of HAEC layer were measured under normal and activated conditions. To activate the HAEC, 10 ng/ml recombinant human TNF-α (R&D Systems, Minneapolis, MN) in complete medium was added to the apical surface of the HAEC, and the cells were analyzed at 1 and 24 h incubation. These times were selected in order to study cells behavior at both early and late time points. Samples treated for 24 h with Triton X-100 (1%, v/v) (Fisher Scientific, Pittsburgh, PA) were used as a negative control (NC) for cell death, and samples in complete media was used as a positive control (PC).

Viability was measured using CellTiter-Blue® assay (Promega, Madison, WI) following the manufacturer's protocol (Fig. 5). This assay measures cellular metabolism by measuring the conversion of the dye resazurin to the fluorescent product resorufin, and only viable cells are able to reduce the former to the latter. Fluorescent intensities of the samples were measured using a fluorescent microplate reader (SpectraMax Gemini XS, Molecular Devices, Sunnyvale, CA) at excitation and emission spectra of 560 and 590 nm, respectively, and reported as relative fluorescent unit (RFU). Unit area resistance of the HAEC cultured in the models was also determined by measuring the trans-endothelial electric resistance (TEER) (WPI, Sarasota, FL) following the manufacturer's protocol (Fig. 6). Average relative fluorescent intensities and unit area resistance of the HAEC obtained under normal and activated conditions were subtracted from the negative control values in order to obtain the true cell layer viability and resistance.

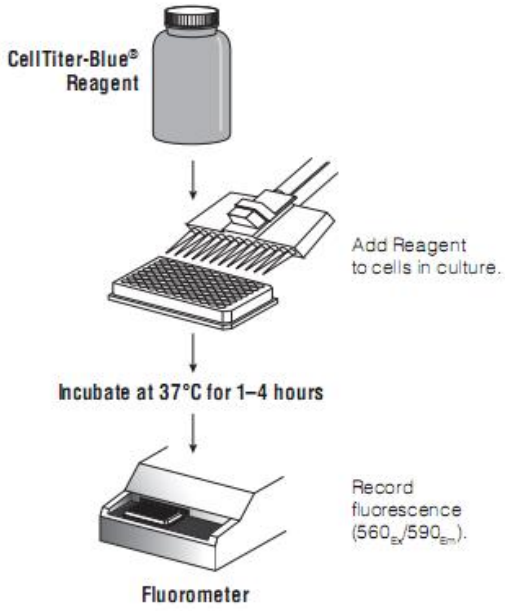

Figure 5. Cell Titer-Blue cell viability assay. Promega Corporation. Technical Bulletin 2009. [cited; Available from http://www.promega.com/tbs/tb317/tb317.pdf]

Furthermore, HAEC grown on collagen coated models were also used as control samples for the endothelium cultured on collagen matrices to investigate if the collagen per se could affect the cell behavior significantly. Average unit area resistance of the confluent HAEC grown on models were reported under normal conditions and subtracted from the unit area resistance of the cell free samples considered as background controls (BG).

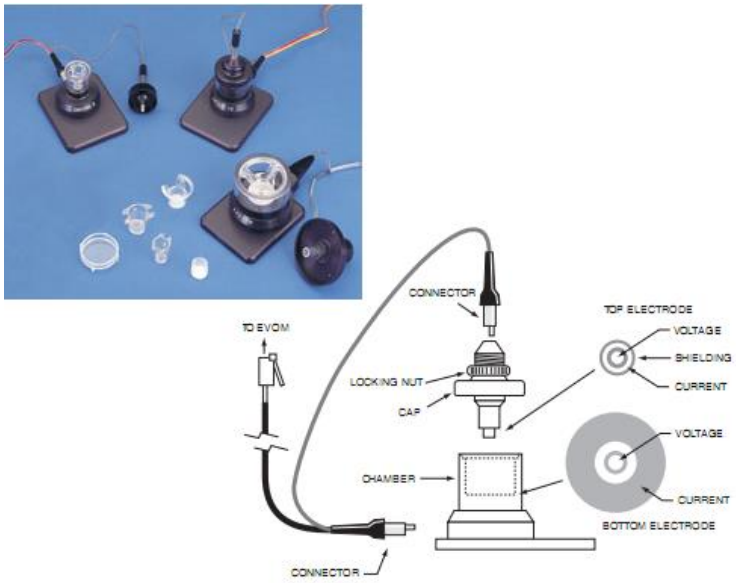

Figure 6. Trans-endothelial electric resistance (TEER) instrument.

Picture source: http://www.wpiinc.com/pdf/endohm-im-041408.pdf

2.2.4 HAEC morphology

HAEC were stained with media containing fluorochrome-conjugated PECAM (5 µg/ml) or isotype antibodies (Biolegend, San Diego, CA) according to standard cell staining protocol (BD Bioscience, San Jose, CA). The stained samples were removed from the inserts, mounted on slides, and the cells nuclei were counterstained with DAPI using ProLong® Gold antifade reagent (Invitrogen, Carlsbad, CA). Samples were examined by confocal microscopy to detect the cells

nuclei and membrane. Images were analyzed using ImageJ software (version 1.49t) to determine the membrane surface areas of 50 cells per three independent samples.

2.2.5 Expression of CAMs and MCP-1 on the endothelial cell surface

The surface expression levels of VCAM-1, ICAM-1, PECAM-1, and MCP-1 were measured under normal and activated conditions. Cells were activated by adding TNF-α to the apical side of the endothelium, as mentioned before, and samples were analyzed after 1, 6, 12, 18, and 24 h incubation time points for the expression of CAMs and MCP-1. HAEC cell culture models incubated without TNF-α served as controls. For flow cytometry, cells were detached from the 2D model using human primary endothelial cell detach kit containing solution of 0.25% trypsin with EDTA (PromoCell), and membrane inserts were washed to collect the lifted cells. To remove the HAEC from the 3D tissue model, the collagen matrices were digested with collagenase D (Roche Applied Science, Indianapolis, IN). Briefly, collagenase D was added on the collagen matrices and incubated at culture conditions for 1-2 h to digest the matrices and the wells were washed to collect all detached cells. Cell suspensions were centrifuged (5 min, 1200 rpm, 4 °C), and immunofluorescence staining was done using anti-human fluorochrome-conjugated CD106 (VCAM-1), CD54 (ICAM-1), CD31 (PECAM-1), MCP-1 or isotype controls (all from Biolegend, San Diego, CA). A flow cytometer (FACSCalibur) was used to analyze the cells within a day of staining and data analyses were performed using FCS Express software (version 3) (Fig. 7). For each sample, uniform population of the endothelial cells were gated using side versus forward scatter plots to exclude dead cells and debris. The Overton subtraction method was used to determine percentage positive (PP) and net mean fluorescent intensity (MFI) of the cells population compared to the isotype controls for each marker [58]. The PP and MFI results of the activated HAEC were normalized to the values obtained for the control samples (media with no TNF-α stimulation).

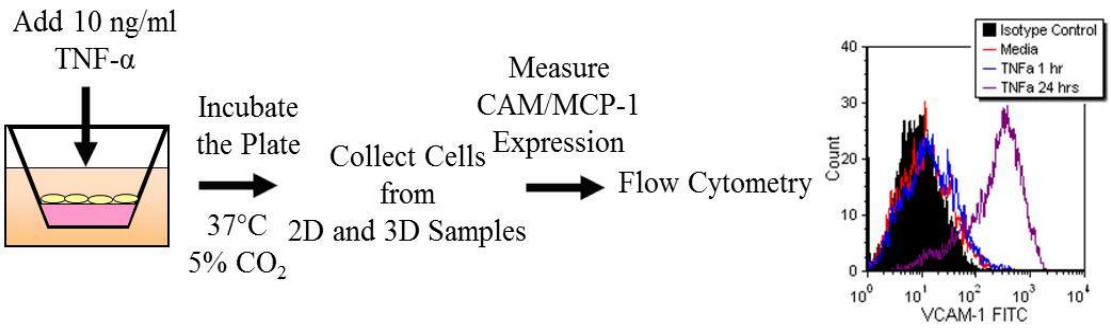

Figure 7. Detecting/measuring CAM/MCP-1 expression on the HAEC.

2.2.6 Release of MCP-1 within the 3D tissue model

The kinetics of MCP-1 release from the HAEC grown in the 2D and 3D models in 12-well inserts were measured under normal and activated conditions. Cells were activated with TNF-α (as described previously), and MCP-1 release was quantified at 1, 6, 12, 18, and 24 h following addition of TNF-α. Culture models incubated without TNF-α were used as controls. To measure MCP-1 release from the 2D and 3D models, media from both the apical and the basal compartments of the endothelium were collected and stored separately at -20 °C. To quantify MCP-1 concentration in the matrix, the collagen matrix was digested by collagenase D (as described before), centrifuged, and the cell-free supernatants were stored at -20 °C. MCP-1 concentration was measured in the collected solutions using a human MCP-1 ELISA kit (BD Biosciences) following the manufacturer's protocol. Then, based on the collagen matrix volume calculations (manuscript in review) and the measured MCP-1 amount in the digested collagen solutions, MCP-1 concentration in the collagen matrices were determined (Fig. 8).

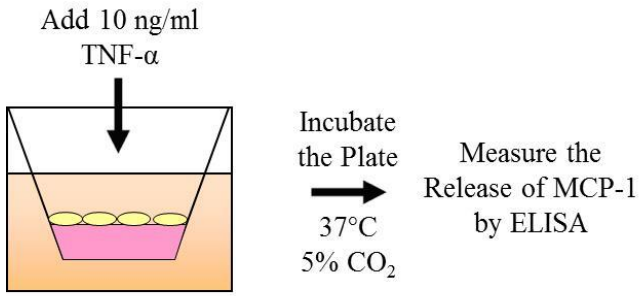

Figure 8. Measuring the MCP-1 kinetics from HAEC in response to TNF-α.

2.2.7 Preparation of monocytes

Human peripheral blood mononuclear cells (PBMCs) were isolated from blood obtained from healthy donors (Oklahoma Blood Institute, Oklahoma City, OK), using a Ficoll-Plaque (GE Healthcare, Uppsala, Sweden) density gradient centrifugation method. Monocytes were negatively selected from the PBMCs using a pan-monocyte isolation kit (Miltenyi Biotech, Auburn, CA) using the manufacturer's protocol, and used immediately for adhesion and migration experiments.

2.2.8 Monocytes adhesion and transendothelial migration

Adhesion and migration of monocytes under normal and activated conditions were studied in both the 2D and 3D models in 12-well inserts. Activation was achieved by adding TNF-α to the HAEC apical layer, and samples were analyzed after 1 and 24 h. At the end of each incubation, culture media were removed from the endothelium apical compartment and human monocytes ($1.5*10^5$ cells/cm^2 in 0.5 ml complete medium) were added. After 2 h, samples were rinsed gently to remove the non-adherent or loosely adherent monocytes, and the entire cell population (HAEC and monocytes) were collected (Fig. 9). Any monocytes that migrated to the endothelial basal layer were also collected. Monocytes that either adhered to or transmigrated across the endothelium were detected by immunofluorescence staining with anti-human CD14 fluorochrome-conjugated antibody or isotype control (BD Biosciences). Analysis was performed within a day of staining. Monocytes population was gated and the Overton subtraction method was used to determine the percentage of CD14 positive cells in each gate compared to the isotype controls [58]. Number of monocytes in gates was calculated based on the total number of events and the percentage of CD14+ cells in each gate. Then, total number of monocytes in each sample

was determined using the number of monocytes in each gate, instrument flow rate, time elapsed for collecting the events, and total initial sample volume.

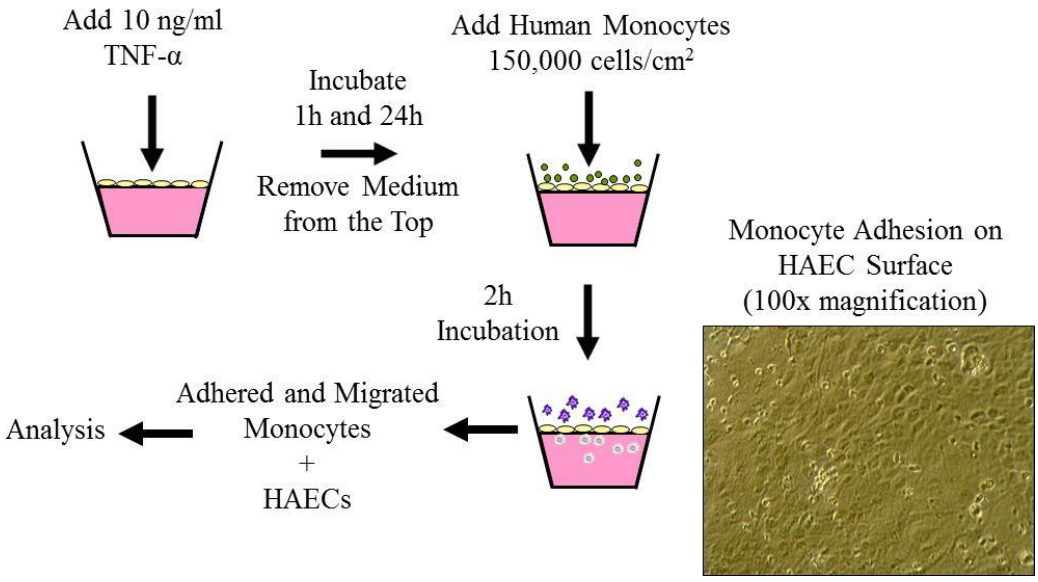

Figure 9. Experimental procedure for examining monocyte adhesion and transmigration in the 3D tissue model.

2.2.9 The effect of MCP-1 on monocytes adhesion and migration

The effect of MCP-1 on monocytes adhesion and migration in the 3D tissue model was also studied using an MCP-1 neutralizing antibody. At the end of 1 and 24 h incubation time point with TNF-α, media was removed from the HAEC apical compartment and was replaced with fresh media containing 750 ng/ml purified anti-human MCP-1 antibody (Biolegend). The samples were incubated for 2 h, the media was removed, and monocytes were added to the apical side of the endothelium. After 2 h incubation, cells were collected and analyzed, as described previously.

2.2.10 Statistical analysis

All experiments were performed in replicate to determine the mean ± standard deviation (SD) of the samples. A nonparametric statistical analysis of Kolmogorov-Smirnov (K-S) test was used to determine if the distribution of cells sizes are equal between independent samples group. Student's t-test was used to determine the significantly different groups among pairs. p value of < 0.05 was considered significant.

2.3 Results

2.3.1 HAEC viability and trans-endothelial electrical resistance

Viability and unit area resistance of the HAEC layer, quantified for both models under normal condition and upon activation by TNF-α for 1 and 24 h, are shown in Fig. 10. To compare the viability of the HAEC, we measured the metabolic activity as an indicator of viability in the cells grown in the models using the Cell-Titer Blue® Assay. No significant difference in cell viability is observed for 2D and 3D models with the addition of TNF-α compared to positive control (PC) samples (Fig. 10A). Furthermore, HAEC viability is lower in the 3D tissue model compared to the 2D model, when cells are activated at early and late time points, but not statistically significant. Our results clearly show that the cells in the novel, 3D tissue model retain viable.

Resistance results, shown in Fig. 10B, indicate that cell layer integrity at normal condition does not alter significantly within 1 h stimulation in 2D and 3D models. However, significant 1.6 and 4.5-fold cell resistance reduction ($p < 0.05$) is observed after 24 h of stimulation compared to the positive control (PC) samples in the 2D and 3D models, respectively. TEER measurements results also shows a significant 1.9, 2.2, and 5.2-fold decrease ($p < 0.05$) in cell resistance for the 3D tissue model compared to the 2D model for positive control samples, and after 1 and 24 h adding TNF-α, respectively. These results suggest that using collagen matrix as the ECM substrate has significant effect on formation of cell-cell junctions and HAEC spreading behavior.

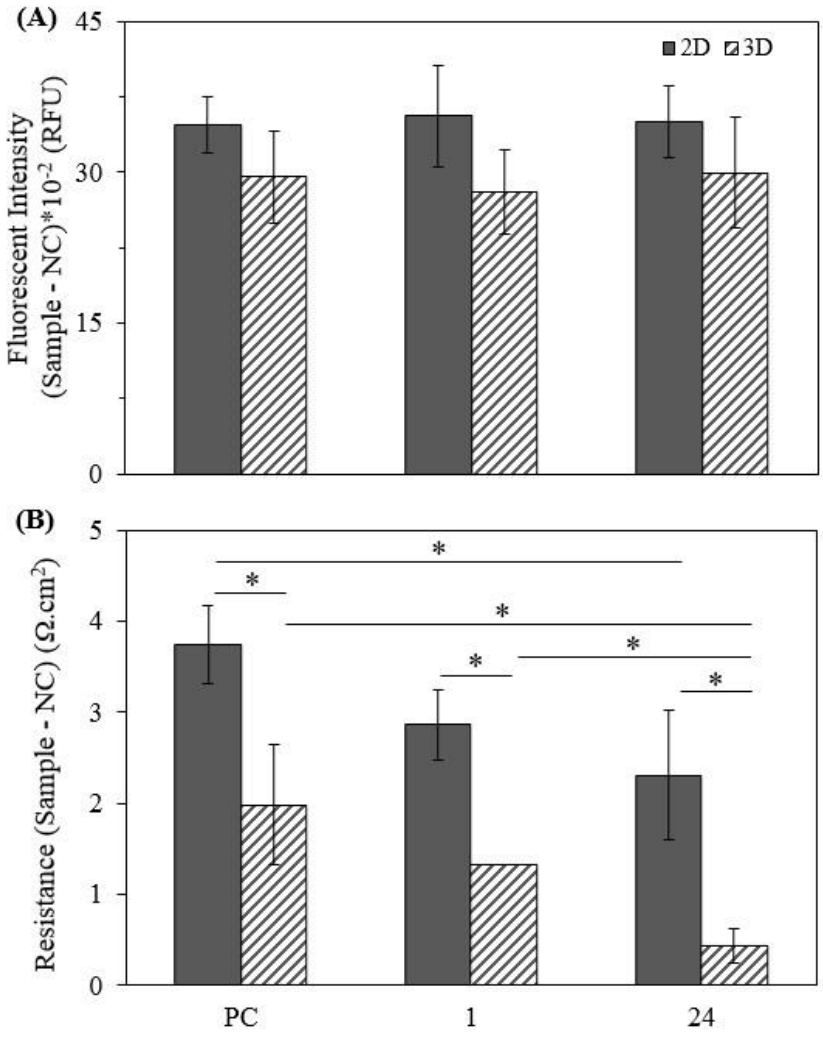

Figure 10. HAEC viability fluorescent intensity measurements (ex/em: 560/590 nm) **(A)** and unit area resistance **(B)** in the 2D and the 3D models under normal condition (positive control: PC) and when the models were activated with TNF-α (10 ng/ml) for 1 and 24 h. Values are presented as mean ± SD of absolute differences compared to the Triton X-100 (1%, v/v) treated samples (negative control: NC); n=3; * indicates p value < 0.05.

The foregoing observations led us to further our understanding of the effect of collagen material per se as opposed to the collagen matrix ECM on HAEC layer unit area resistance. Fig. 11 shows the unit area resistance of the HAEC layer grown on the microporous membrane, collagen coating, and collagen matrix models, quantified by measuring the TEER under normal

condition subtracted from the background (BG) unit area resistance. TEER measurements show a significant 2.1 and 1.6-fold decrease ($p < 0.05$) in cell resistance in the collagen matrix model compared to the microporous membrane and collagen coated samples, respectively. The average unit area resistance of the cells is decreasing as the collagen volume is increasing in the coated and matrix models compared to the 2D model. Therefore, confluent HAEC layer grown in the 3D tissue model had the highest permeability under normal condition.

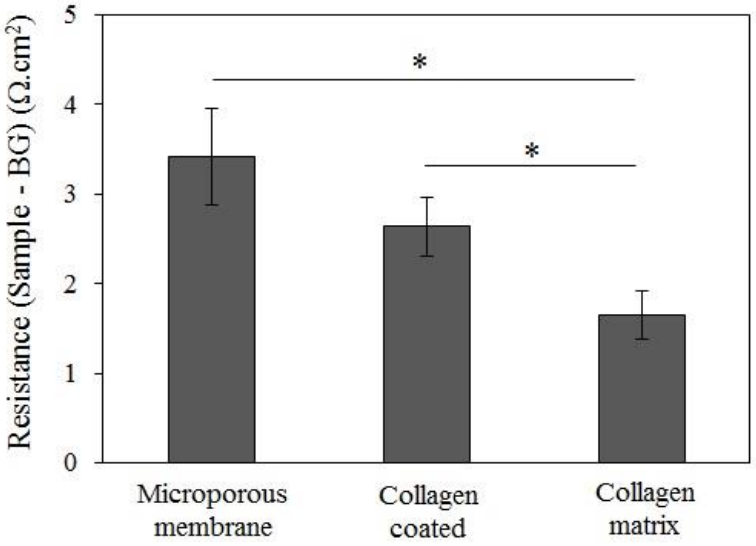

Figure 11. HAEC unit area resistance in the microporous membrane, collagen coated, and collagen matrix models under normal condition. Values are presented as mean ± SD of absolute differences compared to the background (BG); n=3; * indicates p value < 0.05.

The results suggest that endothelium-collagen interaction per se has an influence on cell-cell junctional zones which has decreased the HAEC resistance. Moreover, it is shown that formation of cell-cell junctions pattern not only depends on the interaction of cells and the type of material itself used as the substrate, but also the endothelium resistance varies with using the substrate as subendothelium ECM as opposed to a single layer coating film.

2.3.2 HAEC morphology

In this section, we sought to investigate the influence of subendothelium substrate and ECM on HAEC morphology which led to the observed variations in HAEC unit area resistance in section 2.3.1. Representative images of HAEC cultured on the membrane, collagen coating, and collagen matrices are shown in Fig. 12A. From microscopy analysis, it is observed that HAEC morphology was similar but not identical on the microporous membrane, collagen coated, and the matrices. Generally, HAEC were circular and round shape more like cobblestones and in some cases appeared more elongated in different models. However, quantitative analysis of HAEC sizes in Fig. 12B shows physical variations of cells surface area distribution depending on the interaction between cells and their surroundings substrate.

HAEC grown on the membrane environments exhibit a broad diameter range (22-76 μm) compared to the collagen coated models whereas the diameter range is narrowed down (24-73 μm). However, based on the K-S statistical analysis, HAEC on the collagen coated samples have the same size distribution function as the cells grown on the membrane model. Furthermore, sizes of HAEC grown on the matrices appeared to be more uniformly developed with a smaller diameter range (20-53 μm) and a significant difference ($p < 0.01$) in distribution function compared to the HAEC grown on the membrane and collagen coated models. The significant junctional zone distribution difference of HAEC grown on the collagen matrices compared to the microporous membrane and collagen coated samples suggests that the endothelium unit area resistance ought to be different between the samples which matches the data shown in Fig. 11. These data suggest that not only collagen material itself had an effect on biophysical morphology behavior of HAEC, but also having an ECM under an endothelium altered cells growth and spreading properties.

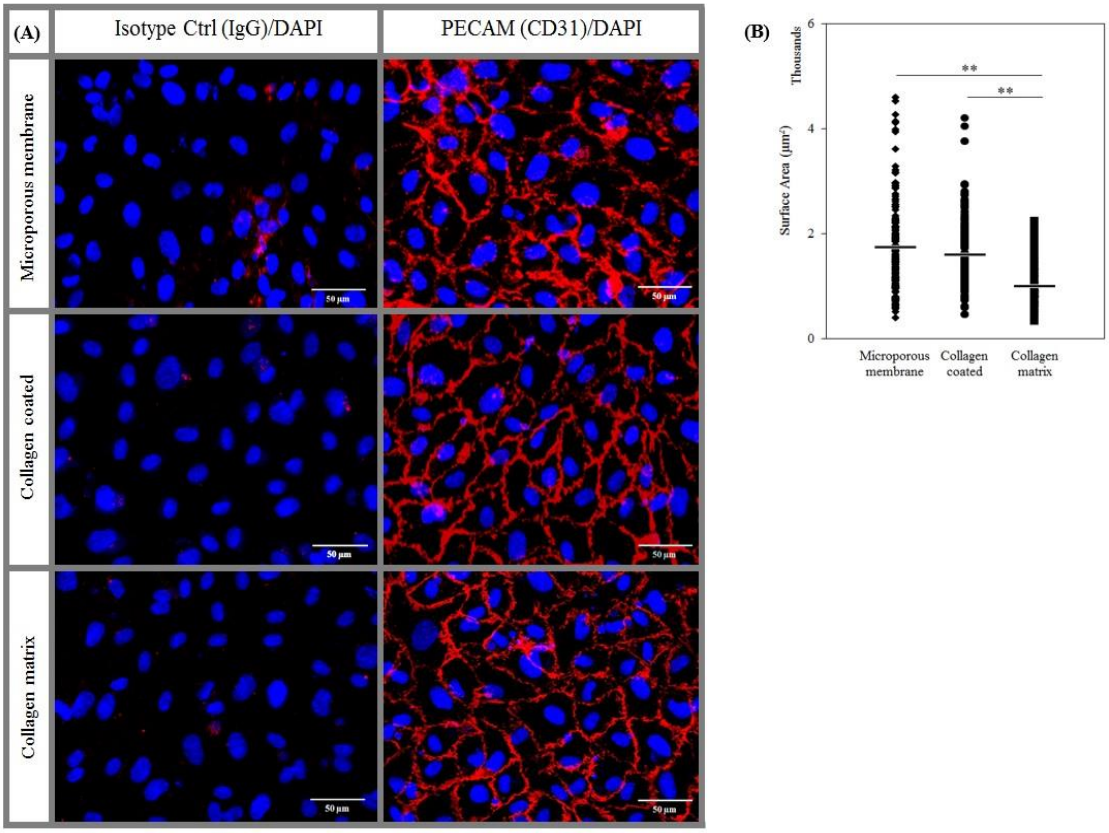

Figure 12. HAEC were immunostained for the nuclei and endothelial marker PECAM-1. **(A)** Confocal microscopy was used to image the aortic endothelial cell shape in microporous membrane, collagen coated, and collagen matrix models. Nuclei and PECAM protein expression were revealed by DAPI staining (blue) and CD31 antibody (red), respectively. All the images were taken at the same magnification of 400× and at the same settings as their staining isotype control IgG. Scale bar, 50 µm. **(B)** Membrane surface areas of 50 cells per sample were analyzed for three independent samples (n=3) using ImageJ software (version 1.49t). Values for each cell are shown in different models and the average surface area is marked with a solid line. ** indicates p value < 0.01.

Furthermore, HAEC packing density was determined according to the microscopy images and reported as 66266 ± 15265, 63252 ± 7468, and 67798 ±12713 cells/cm^2 for microporous membrane, collagen coating, and collagen matrix models, respectively. Although

HAEC size distribution pattern is different on the microporous membrane, collagen coating, and collagen matrix microenvironments, the average cells packing density is not changing significantly. Hence, we expected to get the same cell viability results in different models which correlates to the viability data presented in Fig. 10A.

2.3.3 Expression of CAMs and MCP-1 on the endothelial cell surface

The kinetic and magnitude of CAMs and MCP-1 expression on the HAEC surface was measured for control and TNF-α activated samples by direct immunofluorescence staining and detection by flow cytometry. Results are presented in Fig. 13 as ratio of the net mean fluorescent intensity (MFI) and percentage positive (PP) of cell population in activated samples to the control (media with no TNF-α stimulation).

There was a low expression of VCAM-1 on unstimulated endothelial cells (data not shown), and a significant upregulation of VCAM-1 expression after 24 h TNF-α treatment (15.4-fold increase compared to control). The PP of the cells population expressing VCAM-1 is not changing significantly after 6 h activation for both models. However, the MFI of the VCAM expression is increasing gradually between 6-18 h when it increases significantly after that up to 24 h for both models. At 24 h stimulation by TNF-α, the MFI of VCAM-1 positive cells in the 2D model is significantly higher than cells in the 3D tissue model (2.3-fold, $p < 0.01$).

ICAM-1 is expressed on normal endothelium in control samples (data not shown), but the expression is upregulated after stimulation by TNF-α with a time course similar to that of VCAM-1. Increase of ICAM-1 membrane expression PP reached a plateau after 6 h TNF-α activation. However, the MFI of ICAM membrane expression is increasing in both models. ICAM-1 membrane protein expression was detected to a lesser extent in the 3D tissue model than the 2D model at both early and late time points. It was shown that the MFI expression of ICAM-1 protein were statistically significantly higher in HAEC treated with 24 h TNF-α in 2D models compared to the 3D tissue models (1.9-fold, $p < 0.05$).

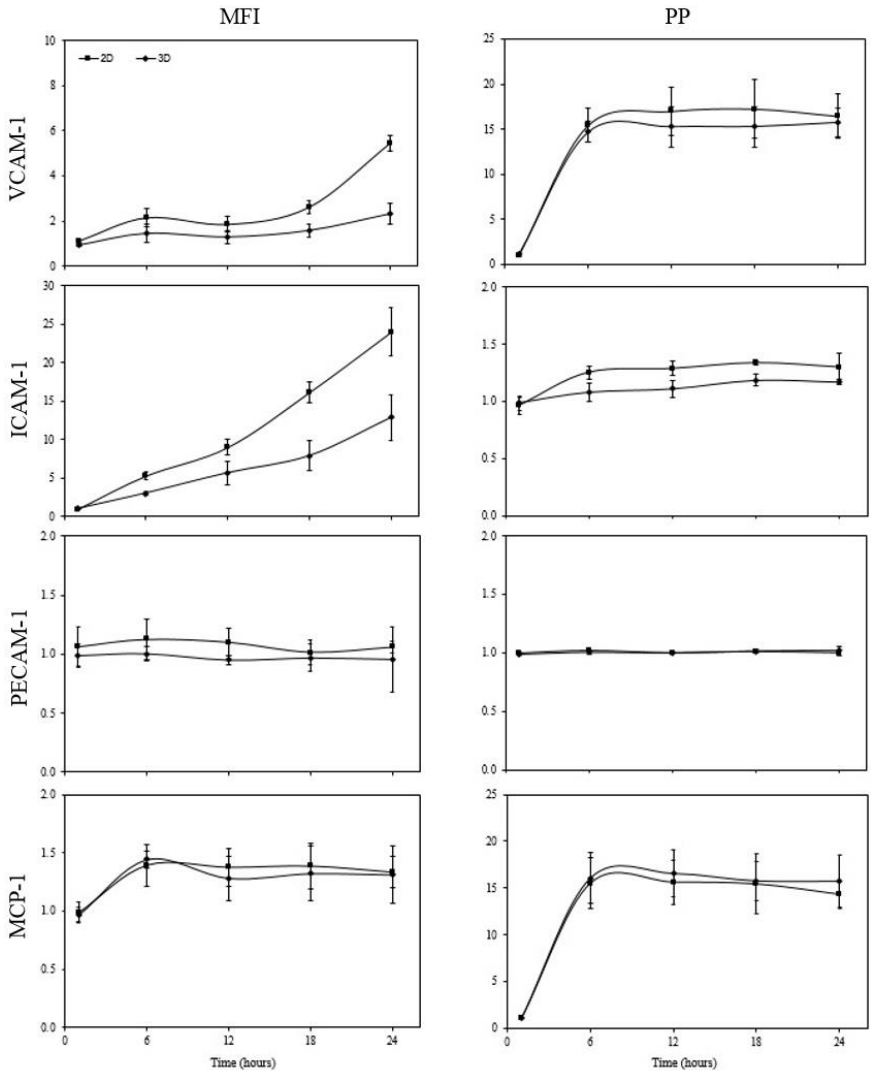

Figure 13. HAEC membrane protein expression flow cytometry analysis of CAMs/MCP-1 in the 2D and 3D models. For each sample, uniform population of the endothelial cells were gated using side versus forward scatter plots to exclude dead cells and debris. The Overton subtraction method was used to determine percentage positive (PP) and net mean fluorescent intensity (MFI) of the cells population compared to the isotype controls for each marker. Results are presented as mean fluorescent intensity (MFI) and percentage positive (PP) of each marker in activated samples normalized to the control samples (media with no TNF-α stimulation); n=3, MFI of HAEC ICAM expression is significantly higher in 2D models compared to the 3D tissue models after 6 h activation with TNF-α (* $p < 0.05$).

It is also worth noting that the increase in PP cells expressing VCAM-1 after activation is significantly higher than the positive cells for ICAM-1 membrane protein compared to the control samples.

PECAM-1 expression localized at cell–cell borders of HAEC confluent monolayers is not upregulated in response to TNF-α compared to the control samples without stimulation. No significant differences of PECAM-1 expression (MFI and PP) were observed on the cells surface between the 2D and 3D models which shows that TNF-α did not have effect on PECAM expression in both models over 24 h activation.

The expression of MCP-1 was observed on the cells surface with not a significant difference between the 2D and 3D models after activation. According to the flow cytometry results, moderate number of HAEC population has expressed MCP-1 after 6 h activation (16.1-fold increase in PP), but with a weak intensity (1.4-fold increase in MFI). The increase of MCP-1 membrane protein expression (both PP and MFI) reached a plateau after 6 TNF-α incubation when it remains unchanged till 24 h stimulation.

The data suggest that TNF-α increases the level of VCAM-1 and ICAM expression on the HAEC surface in both models. And the HAEC from the 2D models have a higher expression of the key CAMs intensity (MFI) and the same expression of MCP-1 associated with monocytes cell migration than the HAEC from the 3D tissue model after 24 h stimulation.

2.3.4 Release of MCP-1 within the 3D tissue model

The kinetic of MCP-1 release from the HAEC over 24 h time point in both the apical and basal side of the HAEC for the 2D and 3D models was measured by ELISA and shown in Fig. 14. The data demonstrate that HAEC had the highest release of MCP-1 in the apical and basal compartments of endothelium after 24 h TNF-α stimulation in both models with a significant difference between the 2D and 3D models at each activation incubation time point.

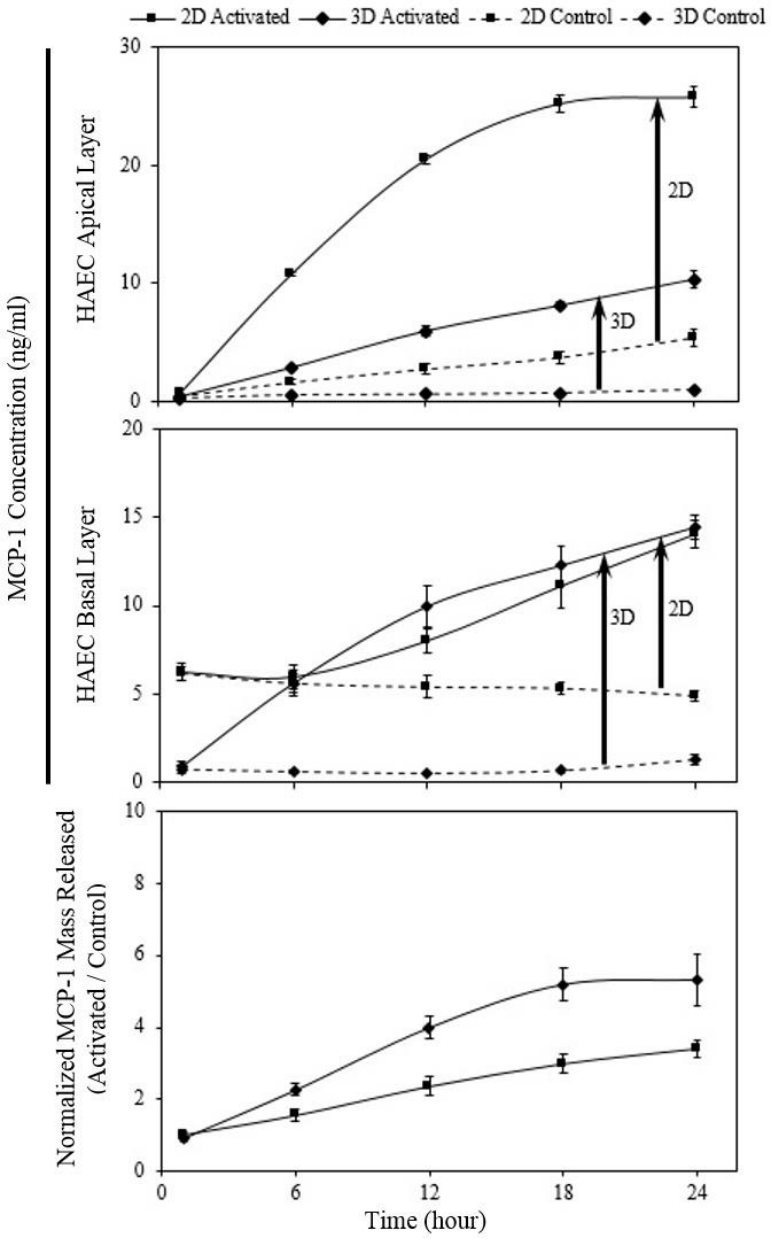

Figure 14. MCP-1 concentration (ng/ml) released from HAEC in the apical and basal of endothelium in 2D and 3D models for TNF-α activated (10 ng/ml) and control (normal condition) samples at different time points. Arrows show concentration elevation from control to activated condition. And ratio of total MCP-1 mass (ng) released from HAEC after treating with TNF-α (10 ng/ml) to MCP-1 mass released in control samples (normal condition) in the 2D model compared to the 3D tissue model at different time points. Values are presented as mean ± SD; n=3, MCP-1 concentration is significantly higher in activated samples compared to control (* $p < 0.05$).

Although the final concentration of MCP-1 in the endothelial basal layer is shown to be identical in the 2D and 3D models, in fact a significant difference in the net release of MCP-1 is observed in the collagen matrix of the 3D tissue model compared to the HAEC basal layer in 2D model. After 24 h activation, HAEC released MCP-1 with 2.9 and 11.2–fold increase compared to the corresponding control samples in the 2D and 3D models, respectively. Accordingly, due to the sample concentrated in the collagen matrix, resulting in an abrogated release into the surrounding media, an earlier detection of MCP-1 release was expected from the 3D tissue model. As it is shown in Fig. 14, there is no significant difference in the MCP-1 concentration released to the basal layer of HAEC in the 2D model after 6 h TNF-α activation compared to the control sample. However, stimulating HAEC in the 3D tissue model for 6 h had a significant effect on MCP-1 release in the collagen matrix beneath the HAEC layer (9.5-fold, $p < 0.01$).

Furthermore, the results display that the ratio of total MCP-1 mass released when HAEC were activated to the control samples increased significantly as the TNF-α incubation time was increasing in both models. Moreover, the normalized MCP-1 amount released is exhibited to be statistically significantly higher in the 3D tissue model compared to the 2D model starting at 6 h stimulation up to 24 h when the ratio was 1.6-fold higher in the 3D tissue model than 2D model ($p < 0.05$). Taken together, these results indicate that having the collagen matrix beneath the endothelium in the 3D tissue model had altered the cells behavior in producing MCP-1 before and after activation which will have an influence on monocytes migration later on.

2.3.5 Monocytes adhesion and transendothelial migration

Total number of monocytes that adhered and migrated across the endothelial cell layer for each model was determined by direct immunofluorescence staining and detection by flow cytometry. The percentage of monocytes that adhered to and migrated through the endothelium after 2 h is presented in Fig. 15. The results show that there are significantly more monocytes transmigration occurred in the 3D tissue model compared to the 2D model after 24 h of

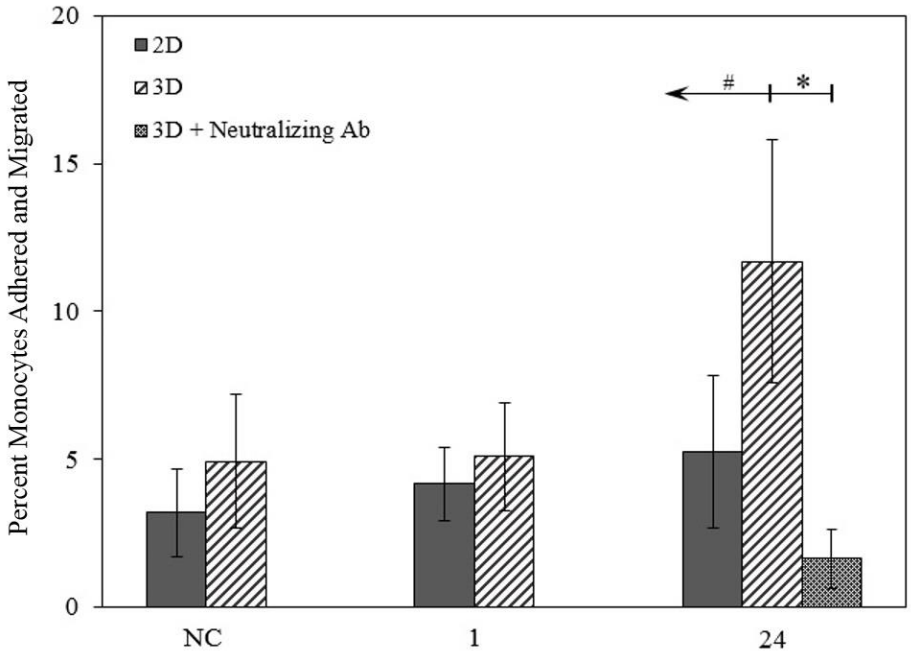

Figure 15. Monocyte adherence and migration across the HAEC layer for each model in response to MCP-1 gradients for control and activated samples. HAEC were treated with 10 ng/ml TNF-α for 1 and 24 h. TNF-α treated 2D and 3D models and 3D tissue models incubated with an excess of MCP-1 neutralizing antibody (neutralizing Ab) were compared. Samples incubated with complete media without TNF-α was used as a negative control (NC). Human monocytes ($1.5*10^5$ cells/cm^2 in 0.5 ml media) were added on the apical layer of HAEC and the samples were incubated at standard conditions for 2 h. At the end of the incubation time, the top surface was rinsed and the number of monocytes that adhered on or migrated through the endothelium was determined. Values are presented as mean ± SD of the percent of attached and migrated monocytes normalized to the initial number of monocytes added to each well; n=3; # and * indicate $p < 0.1$ and 0.05, respectively, for change in percentage of adhered and migrated monocytes.

stimulation (2.2-fold, $p < 0.1$) and the negative control (NC) samples without TNF-α treatment (2.4-fold, $p < 0.1$), which shows the effect of different MCP-1 concentration gradient profile on monocytes migration. An increase in the number of monocytes that migrate across the endothelial layer for the 3D tissue model compared to the 2D model, indicates that MCP-1 influence is greater in the 3D tissue model, due to the MCP-1 haptotactic gradient. The greater number of monocytes for the HAEC in the 3D tissue model can be attributed to the difference in MCP-1 within the collagen of the 3D tissue model compared to the free MCP-1 in the 2D model.

We also studied the specificity of the MCP-1 gradient on the monocyte migration by neutralizing the available MCP-1 with MCP-1 antibody. The results show that there is a significant reduction in the number of monocytes adhered and transmigrated between the anti-MCP-1 antibody-treated samples versus the 24 h activated samples (7.2-fold, $p < 0.05$). Our results clearly show that treatment with the MCP-1 antibody could significantly reduce MCP-1 induced monocytes migration through the collagen matrices.

2.4 Discussion

In this study, an advanced 3D *in vitro* vascular tissue model was introduced as a novel tool to study the early cellular mechanisms involved in atherosclerosis plaque formation. Using this new model, the effect of MCP-1 concentration profile on monocytes migration was determined. The results supported our hypothesis that MCP-1 transport was different in the 3D tissue model than the traditional 2D microporous membrane model, which resulted in a difference in monocytes transendothelial migration between the two models.

Expressed chemokines such as MCP-1 diffuses into the ECM where they can bind to the ECM proteins and maintain, so ECM proteins are important factors for immobilizing chemokines and preserving the profile [40]. Despite of this fact, the nature of the MCP-1 gradient and its effect on monocytes migration has been very difficult to assess in an *in vivo* setting and its mechanism is still not clear and is a very controversial area.

2D cell culture model is widely used to investigate the MCP-1 concentration gradient effect on monocytes migration. Endothelial cells are grown on a thin, microporous membrane, the MCP-1 is added to the aqueous media below the membrane, and monocytes are added to the apical surface of the endothelial layer. MCP-1 is added to both the apical and basal side of endothelium for chemotactic control [90]. Monocytes moved across the pores toward the MCP-1 solution and transmigration of the cells was observed [88]. The number of transmigrated monocytes across the endothelial cell layer and the microporous membrane is counted for different concentrations of MCP-1 and different time points [92]. This model may not adequately predict *in vivo* cell behavior due to the lack of the third dimension which is an important factor in many physiological conditions. Interaction between cells and the below matrix and also the cell migration microenvironment condition are the most important issues that have to be considered in cell culture studies which are not achievable in 2D models. In order to address these issues, subsequent studies have proposed some alternatives as a development of 3D tissue models in laboratories [41, 100]. In this study, 3D tissue model is introduced as a tool to study monocytes transendothelial migration within the ECM. The 3D tissue model consisting of a type I collagen matrix would be a better experimental model to mimic the ECM as it is a major constituent of many tissues that make it useful for many model applications, and it can be obtained in a pure form without mixture of other bioactive ECM proteins which will simplify the experiment and the model [91]. It is more likely to have ECM below the endothelial layer, so the secreted chemokines such as MCP-1 and its corresponding profile can concentrated as a fluid phase or bound to the beneath matrix compound [41]. The 3D tissue model provides the added dimension that is important for the creation of a diffusive concentration gradient formed in the ECM, which is responsible for the control of many cellular mechanisms. Such a 3D tissue model can be used *in vitro* cellular model to construct cell-immunity model [100]. After passing across the endothelial layer monocytes can continue migration via chemoattractants [100] known as MCP-1 [66] in the beneath space.

In this study, we showed that there were significant differences in HAEC response to TNF-α and monocytes transendothelial migration between the 2D and 3D models. Significant differences in HAEC response included the expression of CAMs and the trans-endothelial electric resistance in response to TNF-α stimulation. The HAEC from the 2D models had a greater expression of the key CAMs associated with monocytes cell migration than the HAEC from the 3D tissue models. Significant differences in monocytes transendothelial migration between the 2D and 3D model showed that overall there is greater transendothelial monocytes migration in the 3D tissue model compared to the 2D model. An increase in the number of monocytes that migrate across the endothelial layer for the 3D tissue model compared to the 2D model indicates that MCP-1 influence is greater in the 3D tissue model, possibly due to the haptotactic influence, and that other factors may be driving cell migration in the 2D model.

Findings from comparing the two models contribute to a better understanding of how cells behave in 2D versus 3D models and the development of improved experimental models. Proposed mechanisms can be used to target the MCP-1 involved during the inflammation with highly specific therapeutic strategies. A long term goal of our research group is utilizing the advanced 3D tissue model to test preventative and therapeutic interventions of atherosclerosis.

Overall, the 3D tissue model is utilized in this project to characterize cellular adhesion molecules (CAMs) and to target one specific chemokine marker (MCP-1) that are critical participants in the transmigration of monocytes involved during the formation of the atherosclerosis lesion. The effect of MCP-1 local concentration gradients on monocytes migration is investigated using the 3D tissue model. HAEC behavior (the CAMs and the chemokine expression) and transport properties (MCP-1 release profile) is also studied between the 2D and the 3D models. Differences between two models characteristics, such as MCP-1 concentration gradients and cell behavior, and their effect on monocytes migration, i.e., the effect of diffusive gradients in a 3D environment compared to a 2D model, will help us to have a better understanding of underlying mechanisms in atherosclerosis.

In conclusion, we have shown that kinetics and the level of CAMs expression in the 2D model is different from the 3D tissue model which has an effect on monocytes adhesion and transmigration through the endothelial layer between the two models. This 3D tissue model consisting of a collagen matrix would be a better alternative experimental model to mimic the subendothelial ECM. Such a 3D tissue model provides the added dimension that is crucial for the creation of diffusive concentration gradients which is an important factor in many physiological conditions. So this 3D tissue model can be used as an effective tool for studying the monocytes transendothelial migration through the endothelial layer. The concentration gradient formed in the 3D tissue model is distinctly different compared to the one in the 2D model, where the secreted factors from the endothelial cells dissolve quickly into the surrounding media. Furthermore, the 3D tissue model provides a highly controllable micro-environment for investigating cellular interactions and responses [91]. Apart from this advantage, when focusing on the transmigration of monocytes, this matrix can also provide an area for monocytes to localize and differentiate into macrophages after the transendothelial migration [97]. This latter property of the 3D tissue model makes it applicable as a testing device for many diseases like atherosclerosis.

Many questions still remain about the expression of MCP-1 from endothelial layer and its concentration profile in subendothelial tissue. More studies in this area will lead to the development of an improved *in vitro* model that exhibits native characteristics of *in vivo* in order to study transendothelial monocytes migration associated with MCP-1 profile and inflammatory conditions. Furthermore, as the next phase of this research, we expect utilizing the developed 3D tissue model to develop a second generation mathematical model that describes MCP-1 transport within the 3D model, which will include a source term of MCP-1 production from the HAEC in response to TNF-α and the binding reaction of MCP-1 to the collagen matrix. Validating the mathematical model by comparing the obtained numerical results to the experimental measurements of MCP-1 in the 3D tissue model and determining any correlation to monocytes migration would also be conducted. With the completion of ongoing future phases, an advanced

in vitro tissue model will be developed and can be used to study inflammation in atherosclerosis-associated monocyte migration diseases.

CHAPTER 3

A Mathematical Model to Describe the Release of Monocyte Chemoattractant Protein-1 from Human Aortic Endothelial Cells and the Transport through a Three-Dimensional Collagen Matrix

3.1 Introduction

Atherosclerosis is an inflammatory disease that is initiated by the accumulation of lipid substances in the subendothelial layer of major arteries and followed by adhesion and transmigration of monocytes and lymphocytes to the extracellular matrix (ECM) [4-12]. The end state of the monocytes after transendothelial migration is dependent on many factors, such as the specific tissue involved in the process, the type of stimulus, and the formation of chemotactic concentration gradients in the tissue. The adhesion and transmigration process involves several steps and is mediated by bioactive molecules named chemotactic cytokines (chemokines) [17, 36-40]. Chemokines can form concentration gradients that are free (fluid phase) or bound (immobilized) components [41-48] in the ECM. Monocyte chemoattractant protein-1 (MCP-1) is expressed highly in atherosclerotic lesions in the early stage of atherosclerosis and facilitates monocytes trafficking across the endothelial cell layer [53-55, 57-59]. MCP-1 recruits monocytes to sites of tissue injury, infection, and inflammation via its concentration gradient [63-67, 89]. The absence of MCP-1 in a murine model is also shown to decrease the formation of atherosclerotic lesion [61, 62].

These findings suggest that MCP-1 plays an important role in atherosclerosis formation. Having a better understanding of the underlying mechanisms involved in the role of MCP-1 in controlling monocytes migration will help to identify targets to prevent the atherosclerotic plaque formation.

Previous studies have used two-dimensional (2D) experimental systems to investigate the effect of chemokines on monocyte migration [65, 88-90]. Traditional 2D systems may not be suitable predictors of what occurs in more complex three-dimensional (3D) systems, like those within the human body [91]. The 2D cell culture model is adequate for showing a response of monocytes to a chemokine that has formed a concentration gradient of free proteins across the endothelial cell layer; however, the 2D system cannot be used to examine bound chemokine concentration gradients that form within the tissue *in vivo* [17, 36, 40, 44, 47, 48, 71, 72, 93-96]. In the 2D system, endogenous MCP-1 released by the cells to the surrounding liquid media is diluted, quenching the chemoattractant effect.

A better alternative experimental model is a 3D model consisting of a matrix to mimic the subendothelial ECM. The major advantage of the 3D model is that the third dimension provides the supplementary space that is significant for the creation of diffusive concentration gradients in the ECM. During analysis of a 3D system consisting of a collagen matrix without cells, a binding reaction between MCP-1 and the collagen matrix was discovered, which shows that in addition to a gradient of free MCP-1, a gradient of collagen-bound MCP-1 may be formed in the collagen matrix as well [98]. Due to the low concentrations (pg-ng per ml range), there is no technique available to quantify such gradients inside the collagen matrix.

In this study, a three-dimensional (3D) *in vitro* vascular tissue model was created in order to provide the added dimension required to form diffusive concentration gradients of endogenous MCP-1. The 3D tissue model consists of Human Aortic Endothelial Cells (HAEC) grown on the surface of a collagen matrix, to mimic the vascular endothelium and the subendothelial ECM, respectively. The main objective of this study was to derive a mathematical model to predict the

MCP-1 concentrations at various time points and locations within the collagen matrix of the 3D model. The unsteady-state transport model includes a source term to describe MCP-1 production from the HAEC and a binding reaction term to describe the interaction of MCP-1 with the collagen matrix. The release of MCP-1 from the HAEC in the 3D model, under normal cell culture conditions and in response to an inflammatory stimulus was determined. Tumor necrosis factor-α (TNF-α) was used as an immunologically activator to mimic inflammation that occurs in the early stages of atherosclerosis.

The mathematical model analysis will provide new information about formation of the free and bound MCP-1 concentration profile in the ECM. Then, the concentrations profile can be related back to the monocytes transendothelial migration associated with inflammation involved in the early stages of atherosclerosis.

3.2 Methods

3.2.1 Cell culture

Human Aortic Endothelial Cells (HAEC) and endothelial cell basal medium were purchased from PromoCell, Heidelberg, Germany. HAEC were cultured in 75 cm^2 flasks and incubated at standard conditions (37 °C, humidified atmosphere of 5% CO_2) and used at 90% confluence.

3.2.2 Preparation of the 3D *in vitro* vascular tissue model

The 3D *in vitro* tissue model was constructed in 12-well format ThinCert Transwells® (Greiner Bio-one, Frickenhausen, Germany) as described in the previous protocols [97, 98]. Briefly, the collagen matrix was coated with fibronectin (Biomedical Technologies, Stoughton, MA) and seeded with HAEC ($7.5*10^4$ cells/cm^2). The cells were incubated and used for experiments one day post-confluence. A schematic diagram of the 3D tissue model is shown in Fig. 16A.

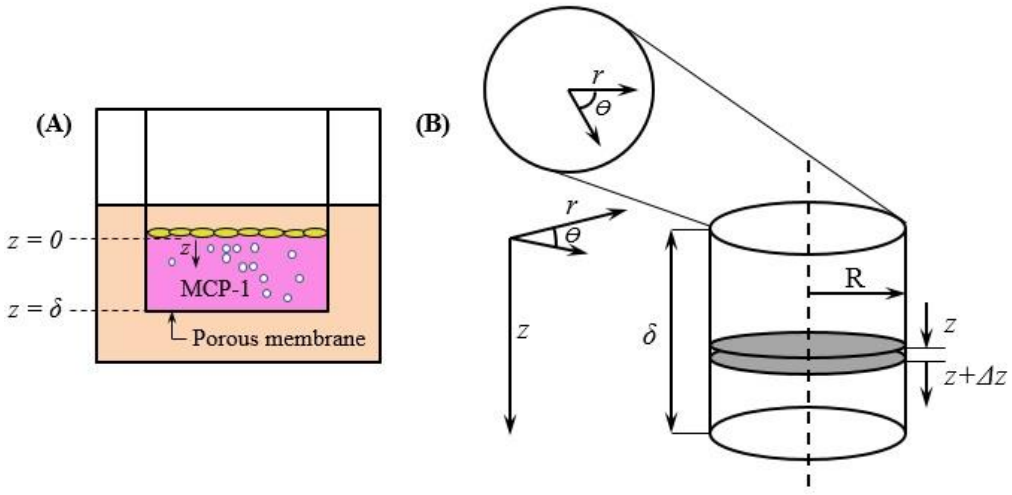

Figure 16. **(A)** Schematic side view of 3D *in vitro* tissue model containing collagen matrix to represent an extracellular matrix (ECM) and an endothelium on top. The model was used to describe the release of monocyte chemoattractant protein-1 (MCP-1) from Human Aortic Endothelial Cells (HAEC) and the subsequent diffusion and transport through the ECM. **(B)** One dimensional unsteady-state axial diffusion in cylindrical coordinate model used to describe the diffusion of released MCP-1 in the 3D tissue model.

3.2.3 MCP-1 and collagen binding reaction

The rate constant for the reaction between MCP-1 and collagen was determined experimentally, by adding a known concentration of recombinant human CCL2/MCP-1 (R&D Systems, Minneapolis, MN) to a collagen matrix and measuring the amount that binds to the collagen after set incubation times. Samples of the collagen matrix were prepared in a solid 96-well plate (Greiner Bio-one, Frickenhausen, Germany). Solutions of MCP-1 at the following concentrations were prepared in complete medium (endothelial basal media with growth factors, PromoCell) and added to the top of the collagen matrix: 10, 25, and 50 ng/ml. The samples were incubated at culture conditions for 1, 6, 12, and 24 h to allow for MCP-1 to bind to the collagen matrix. After incubation, the complete media was collected and the collagen matrix was washed five times with the complete medium to ensure that all free MCP-1 is removed completely from

the collagen matrix. For each wash, fresh complete medium was added to the top of the collagen matrix and incubated for 1 h. The concentration of MCP-1 in the collected samples was measured by a commercially available human MCP-1 ELISA kit (BD Biosciences, San Jose, CA), following the manufacturers protocol. Based on the measured MCP-1 concentrations and having the collagen matrix volume calculations (manuscript in review), MCP-1 concentration in the collagen matrices were determined.

3.2.4 The production rate of MCP-1 from the endothelial cells during the growth phase

To determine the production rate of MCP-1 from HAEC during the growth phase, samples were analyzed for MCP-1 release after 2, 4, and 6 days post seeding HAEC on the collagen matrices during endothelium growth phase. To measure MCP-1 release from HAEC in the 3D tissue models, media from both the apical and the basal compartments of the endothelium were collected and stored separately at -20 °C. To quantify MCP-1 concentration in the matrix, collagen matrices were digested by using collagenase D (Roche Applied Science, Indianapolis, IN). Briefly, collagenase D was added on the collagen matrices and incubated at culture conditions for 1-2 h to digest the matrices. Digested samples were centrifuged and the cell-free supernatants were stored at -20 °C. MCP-1 concentration was measured in the collected solutions using a human MCP-1 ELISA kit following the manufacturer's protocol and the MCP-1 concentration in the collagen matrices were determined.

3.2.5 The production rate of MCP-1 from the endothelial cells during the activation phase

To determine the MCP-1 production rate, the total concentration of MCP-1 released at 1, 6, 12, 18, and 24 h before and after activation was determined. MCP-1 concentration in the apical and basal layer of HAEC were measured by ELISA, using the manufacturer's recommended protocol as described in section 3.2.4.

3.2.6 Statistical analysis

MCP-1 concentrations are reported as mean ± standard deviation (SD) of triplicate samples. Student's t-test was used to determine if there are significant differences in the MCP-1 measured concentrations among the pairs. A p value of < 0.05 is considered significant.

3.3 Model development

The release of MCP-1 from the endothelial cell layer and subsequent diffusion through the collagen matrix was modeled as one dimensional unsteady-state diffusion in cylindrical coordinates, as shown in Fig. 16B. The cross sectional area and pore size of the membrane well used in this study were 1.13 cm^2 and 8.0 μm, respectively. The equation of continuity, along with experimental data, was used to derive a mathematical model that can be used to estimate MCP-1 concentration gradients within the 3D tissue model. The concentration gradients within the 3D tissue model are formed by diffusion of released MCP-1 from the endothelial cell surface into the collagen matrix through the bottom chamber. The binding reaction between MCP-1 and the collagen matrix can be displayed as:

$$F{\bullet}M + S \longrightarrow B{\bullet}M$$

Where $F{\bullet}M$ is the free MCP-1, S is a binding site in the collagen matrix, and $B{\bullet}M$ is a bound MCP-1 to the collagen binding site. Diffusion of MCP-1 in the 3D tissue model was modeled as unsteady-state diffusion in one dimension [44] as shown in Fig. 16. The equation of continuity was used to derive a mathematical model that can be used to estimate MCP-1 concentration gradients within the 3D tissue model.

3.3.1 Assumptions

The following assumptions were made to simplify the equation of continuity:

1) Solutions above and below the collagen matrix were well-mixed, so there are no MCP-1 concentration gradients in the apical side of endothelium and below the membrane compartment. In order to test the validity of this assumption, the value of diffusion coefficient of MCP-1 in the water was compared to the diffusion coefficient obtained in the previous study [44]. MCP-1 diffusion coefficient in water was estimated previously [47]. Diffusion coefficient of bioactive molecules that are in the same family of MCP-1 was also reported by Fluery et al [48]. It was found that MCP-1 diffusion in water is faster than in the collagen matrix. Diffusion coefficients of molecules with various molecular weights also showed higher values in normal compare to free diffusion in water [49]. This finding suggests that MCP-1 diffuses more quickly in the top and bottom reservoirs than in the collagen matrix.

2) The MCP-1 concentration at the top surface of the collagen matrix is equal to the concentration of the top reservoir, and the MCP-1 concentration at the bottom surface is equal to the concentration of the bottom reservoir.

3) The volumes of the top and bottom reservoirs are constant.

4) The effective diffusive coefficient of MCP-1 is constant and not a function of concentration, because the MCP-1 concentration is very small (in pg/ml - ng/ml level range).

5) The change in the MCP-1 concentration has a negligible effect on the total concentration of the system, since the MCP-1 concentration range is very small (in pg/ml - ng/ml level). So, the total concentration is constant.

6) Binding reaction rate depends only on the concentration of MCP-1. Since the concentration of collagen is significantly higher than MCP-1 concentration level range (pg/ml - ng/ml), it is assumed that the collagen concentration is not changing significantly compare to the MCP-1 concentration. Thus, the concentration of collagen is considered as a constant value.

7) The migration of MCP-1 through the collagen matrix is due to the diffusive concentration gradients only not convective mass transfer, since the system is static.

8) The diffusion gradient is assumed to be only in *z*-direction, the perpendicular direction to the endothelial layer. There is no radial (*r*-direction) or angular (θ-coordinate) MCP-1 concentration gradient, due to the system symmetry in the collagen matrix cylinder shape model.

9) The effect of MCP-1 mass transfer across the thin, polycarbonate membrane is negligible in comparison with the diffusion through the collagen matrix, because (i) the thickness of the membrane is significantly less than that of the collagen matrix and (ii) the pore size of the membrane is few orders of magnitude larger than the size of MCP-1 molecules (4 nm diameter).

10) Binding of MCP-1 to the wall of the membrane well is neglected. The system is incubated with basal media containing endothelial growth factors overnight prior seeding the cells. The endothelial growth factors include fetal calf serum (FCS) that can act as a blocking protein for the non-specific bindings in the system.

11) The curvature of the top surface of the collagen matrix due to meniscus formation during the gelation process is neglected. Because the membrane radius is significantly higher than the collagen thickness (1.8-fold), the resulting curvature can be neglected.

3.3.2 Governing equations

By applying the assumptions, listed in section 3.3.1, to the equation of continuity, the mathematical model becomes:

$$\frac{\partial C_{F.M}(z,t)}{\partial t} = D_{M|C}\left(\frac{\partial^2 C_{F.M}(z,t)}{\partial z^2}\right) + R_{F.M}(z,t) \qquad \text{Eq. 1}$$

Where $D_{M/C}$ is the diffusive coefficient of MCP-1 through the collagen matrix (0.108 mm^2/hr) [44]; $R_{F.M}$ is the reaction rate term; $C_{F.M}$ is the mass concentration of free MCP-1 in the collagen matrix; *t* is time, and *z* is the distance from the top surface of the collagen. The reaction rate term is used to describe the rate of conversion of free MCP-1 in the collagen matrix to the bound MCP-1 form. According to our previous study, there is no loss of MCP-1 during the current

experimentation time period according to our previous study [46]. The consumption rate of MCP-1 is shown in Eq. 2.

$$R_{F.M}(z,t) = -K_b C_{F.M}(z,t)^{\alpha} \quad \text{Eq. 2}$$

In Eq. 2, $R_{F.M}$ is the rate term; $C_{F.M}$ is the concentration of free MCP-1 in the collagen matrix; K_b is the rate constant for the binding; α is the order of the reaction; t is time; and z is the distance from the top surface of the collagen (Fig. 1A).

By substituting Eq. 2 into Eq. 1, the model equation becomes:

$$\frac{\partial C_{F.M}(z,t)}{\partial t} = D_{M|C}\left(\frac{\partial^2 C_{F.M}(z,t)}{\partial z^2}\right) - K_b C_{F.M}(z,t)^{\alpha} \quad \text{Eq. 3}$$

This equation determines the concentration of free MCP-1 within the 3D tissue model at various time points and locations.

The equation of continuity was used to develop a mathematical model that represents the bound MCP-1 concentration profile in the collagen matrix. As opposed to free MCP-1, which could diffuse through the matrix, bound MCP-1 is assumed to be fixed inside the collagen matrix, due the binding of free MCP-1 and the collagen binding site. Therefore, the equation of continuity for bound MCP-1 contains the accumulation and the rate of production terms and is shown in Eq. 4.

$$\frac{\partial C_{B.M}(z,t)}{\partial t} = R_{B.M}(z,t) \quad \text{Eq. 4}$$

In Eq. 4, $C_{B.M}$ is the mass concentration of bound MCP-1 in the collagen matrix as a function of time and location in the z-axis, and $R_{B.M}$ is the MCP-1 binding reaction rate term. The production rate of bound MCP-1 is equal to the negative value of the consumption rate of free MCP-1, as shown below in Eq. 5,

$$R_{B.M}(z,t) = -R_{F.M}(z,t) = K_b C_{F.M}(z,t)^{\alpha} \quad \text{Eq. 5}$$

Combing Eq. 4 and 5, the mass balance equation of the bound MCP-1 in the collagen matrix becomes:

$$\frac{\partial C_{B.M}(z,t)}{\partial t} = K_b C_{F.M}(z,t)^{\alpha} \qquad \text{Eq. 6}$$

In order to solve Eq. 3 and 6, initial conditions for $C_{F.M}$ and $C_{B.M}$ and boundary conditions for $C_{F.M}$ are required.

3.3.3 Initial and boundary conditions

To solve Eq. 3 and 6 for the 3D tissue model, the initial and boundary conditions are shown in Eq. 7 and 8, respectively.

Initial conditions:

$$C_{F.M}(z,0) = \frac{\partial C_{i.F.M}}{\partial z}$$
$$C_{B.M}(z,0) = \frac{\partial C_{i.B.M}}{\partial z} \qquad \text{Eq. 7}$$

Boundary conditions:

$$\text{At} \quad z = 0 \quad t > 0 \quad \frac{\partial C_{F.M}(0,t)}{\partial t} = \left(\frac{D_{M|C} A_{surface}}{V_{top\,reservoir}}\right)\frac{\partial C_{F.M}(0,t)}{\partial z} + R_{p.a}$$
$$\text{At} \quad z = \delta \quad t > 0 \quad \frac{\partial C_{F.M}(\delta,t)}{\partial t} = -\left(\frac{D_{M|C} A_{surface}}{V_{bottomreservoir}}\right)\frac{\partial C_{F.M}(\delta,t)}{\partial z} \qquad \text{Eq. 8}$$

For the initial conditions shown in Eq. 7, $C_{i.F.M}$ and $C_{i.B.M}$ are the initial concentrations of free and bound MCP-1 in the collagen matrix before endothelial cell activation, respectively. For the boundary conditions shown in Eq. 8, A is the surface area of the top or bottom surface of the collagen; V is the volume of the top and bottom chambers; δ is the thickness of the collagen matrix; and $R_{p.a}$ is the production rate of MCP-1 from the endothelial cells (source term) at each time point of activation.

3.3.4 Free and bound MCP-1 concentration profile during the endothelial cells growth phase

The amount of MCP-1 released from the HAEC in the 3D tissue model during cell proliferation was measured in order to determine the initial concentration profile of free ($C_{i.F.M}$) and bound ($C_{i.B.M}$) MCP-1 in the collagen matrix (prior to activation). The equations of continuity (Eq. 3 and 6) were used to develop a mathematical model that represents the MCP-1 concentration gradient in the collagen matrix during the growth phase. For the growth phase, the initial concentration of MCP-1 was zero at time = 0, when HAEC were seeded on top of the collagen matrix.

Initial conditions:

$$\text{At} \quad z \geq 0 \quad t = 0 \quad \begin{matrix} C_{F.M}(z,0) = 0 \\ C_{B.M}(z,0) = 0 \end{matrix} \qquad \text{Eq. 9}$$

The boundary conditions described in the activation phase were modified to the following.

Boundary conditions:

$$\begin{aligned} &\text{At} \quad z = 0 \quad t > 0 \quad \frac{\partial C_{F.M}(0,t)}{\partial t} = \left(\frac{D_{M|C} A_{surface}}{V_{top\,reservoir}} \right) \frac{\partial C_{F.M}(0,t)}{\partial z} + R_{p.g} \\ &\text{At} \quad z = \delta \quad t > 0 \quad \frac{\partial C_{F.M}(\delta,t)}{\partial t} = -\left(\frac{D_{M|C} A_{surface}}{V_{bottomreservoir}} \right) \frac{\partial C_{F.M}(\delta,t)}{\partial z} \end{aligned} \qquad \text{Eq. 10}$$

In the boundary conditions shown in Eq. 10, $R_{p.g}$ is the production rate of MCP-1 from the endothelial cells during the growth phase.

3.3.5 The order of the reaction and the reaction rate constant for MCP-1 and collagen binding

The system was modeled as a batch reactor, and the differential method was used for the rate analysis, as shown in Eq. 11.

$$R_{F.M}(z,t) = \frac{dC_{F.M}}{dt} \quad \text{Eq. 11}$$

The above differential rate model (Eq. 11) was used in combination with the Eq. 2 and the experimental data obtained from section 3.2.3 to determine the order of the reaction (α) and the reaction rate constant (K_b) experimentally.

3.4 Numerical solution

The resulting partial differential mathematical equations were solved in MS-Excel (version 2010) with Visual Basic for Applications (VBA) using the Crank-Nicolson numerical method.

3.5 Empirical solution

The numerical results obtained from solving the differential mathematical equations were fed in MATLAB software (version 8.3) and a curve fitting tool was applied to the data to determine the best 3D curve fit for MCP-1 concentrations at different location within the collagen matrix and different stimulation time point. Obtained equation of MCP-1 concentrations as a function of location and time was integrated over the total location range in the matrix (δ) and the incubation time point to calculate the expected total MCP-1 mass in the collagen matrix at each time point.

3.6 Results

3.6.1 MCP-1 and collagen matrix interaction

Existence of an irreversible binding reaction between MCP-1 and collagen matrix was demonstrated in our previous study (manuscript in review). Briefly, human recombinant MCP-1 (50 ng/ml) was added on top of the collagen matrix and the plate was incubated for 24 h allowing MCP-1 to diffuse in the matrix. Samples were washed ten times in order to remove the free MCP-

1 from the matrices. The amount of free MCP-1 in the solution was measured and a mass balance equation (Eq. 12) was used to determine the amount of remaining MCP-1 in the collagen matrix after each wash. Obtained results showed that the total MCP-1 concentration in the collagen matrix decreased gradually with each wash until the fifth wash where there was no significant change in MCP-1 concentration in the collagen matrix was observed for the remaining washes.

$$C_{j.matrix} = \frac{(C_i - \sum_{j=0}^{n} C_{F.M.j})V_{top}}{V_{matrix}} \quad \text{Eq. 12}$$

In Eq. 2, $C_{j.matrix}$ is the total MCP-1 concentration in the collagen matrix at the end of each washes; C_i is the MCP-1 concentration initially added on top of the collagen matrix; $C_{F.M.j}$ is the free MCP-1 concentration in the top solution at each wash; n is the number of washes; V_{top} is the volume of the solution on top of the collagen matrix, and V_{matrix} is the volume of the collagen matrix.

In the current study, we have used different initial concentrations of MCP-1 (10, 25, and 50 ng/ml) and incubated the samples for 1, 6, 12, and 24 h time points to investigate the kinetic mechanism behavior of the binding reaction as a function of the initial concentration and the reaction time. For each initial concentration, total MCP-1 concentration in the collagen matrices were calculated at each incubation time point and after each wash using the mass balance (Eq. 12) for the total number of five washes and results are represented in Fig. 17.

The results show that total MCP-1 concentration in the collagen matrices is highly dependent on the MCP-1 concentration initially added on the collagen matrices and the matrices incubation time points. It is demonstrated that at low initial concentrations, such as 10 ng/ml, there is no significant increase in the total MCP-1 concentration in the collagen matrix when the incubation time is increasing from 1 to 6 h. The average MCP-1 concentration in the collagen matrix is increasing gradually as the incubation time increases to 24 h where there is a significant change compared to the results after 1 h (2.4-fold, $p < 0.01$). In contrast to 10 ng/ml, when 25

ng/ml MCP-1 was used initially, there is a significant increase in the total MCP-1 concentration in the matrices between 1 to 6 h (1.6-fold, $p < 0.01$) where there is no significant change in the total MCP-1 concentration after that up to 12 h. However, increasing the incubation time from 6 to 24 h, has increased the total MCP-1 concentration in the matrix significantly (1.2-fold, $p < 0.05$). Increasing the initial concentration to 50 ng/ml has increased the total MCP-1 concentration in the collagen matrices, significantly, compared to 25 ng/ml results at each time point ($p < 0.01$). Having 50 ng/ml initial concentration and increasing the incubation time from 1 to 6 h, has increased the MCP-1 concentration in the matrix significantly (1.4-fold, $p < 0.05$) where there is no significant change in the total concentration after that up to 24 h.

Having the concentration of free MCP-1 at the end of each incubation time and after each wash, the concentration of free MCP-1 in each system (total sample volume) after each incubation time period was determined. Furthermore, the concentration of bound MCP-1 in the system was calculated based on the data obtained from Fig. 17. The concentration of free and bound MCP-1 in the system is reported for each initial concentration at different incubation time point and represented in Fig. 18.

It was demonstrated that at low initial concentrations, such as 10 ng/ml, there is no reaction between collagen and MCP-1 up to 12 h and the average total MCP-1 concentration in the collagen matrix is increasing gradually as the incubation time increases to 24 h when there is a significant increase in the concentration of bound MCP-1 compared to 1 h (5.5-fold, $p < 0.05$). However, with increasing the initial concentration to 25 ng/ml, collagen and MCP-1 forms an irreversible binding even after short period of incubation time, such as 1 h. Incubating the collagen matrices for another 5 h has elevated the concentration of bound MCP-1 in the system significantly (1.7-fold, $p < 0.05$). The concentration of bound MCP-1 in the system has not been changed significantly after 6 h up to 24 h.

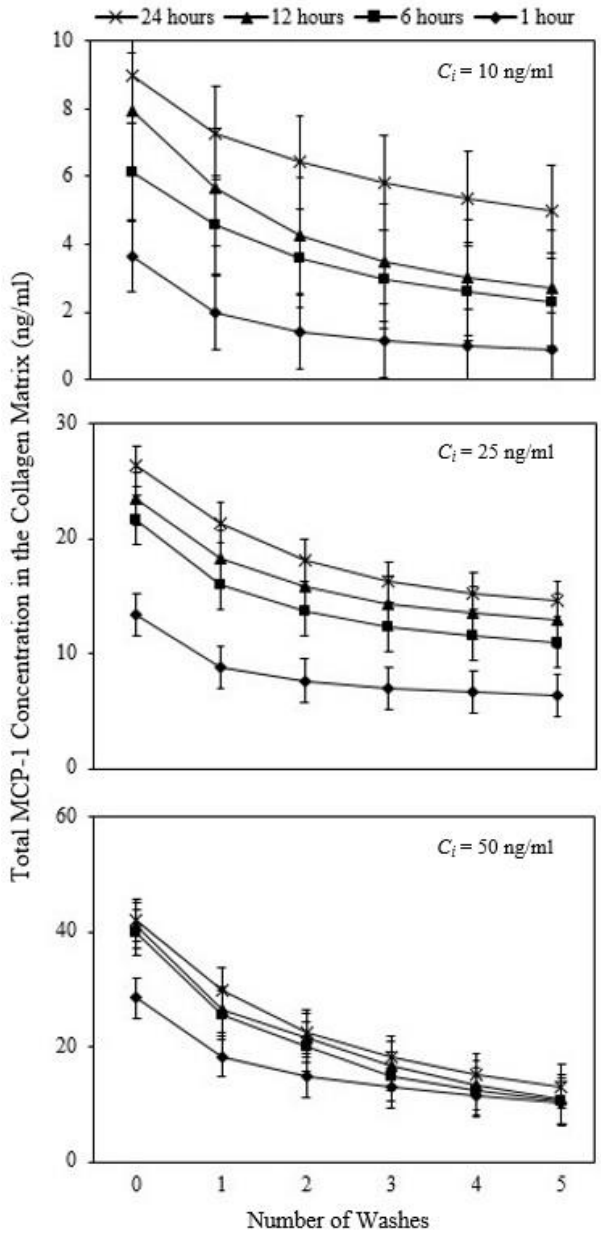

Figure 17. The concentration of MCP-1 (ng/ml) in the collagen matrix at the end of each incubation time and after each washes. Collagen matrices were pretreated with 10, 25, and 50 ng/ml MCP-1 and incubated for 1, 6, 12, and 24 h. The concentration of free MCP-1 in the top solution was measured by ELISA and the mass balance equation was used to determine the remaining total MCP-1 concentration in the collagen matrices (as described in Materials and Methods). Values are presented as mean ± SD; n=3.

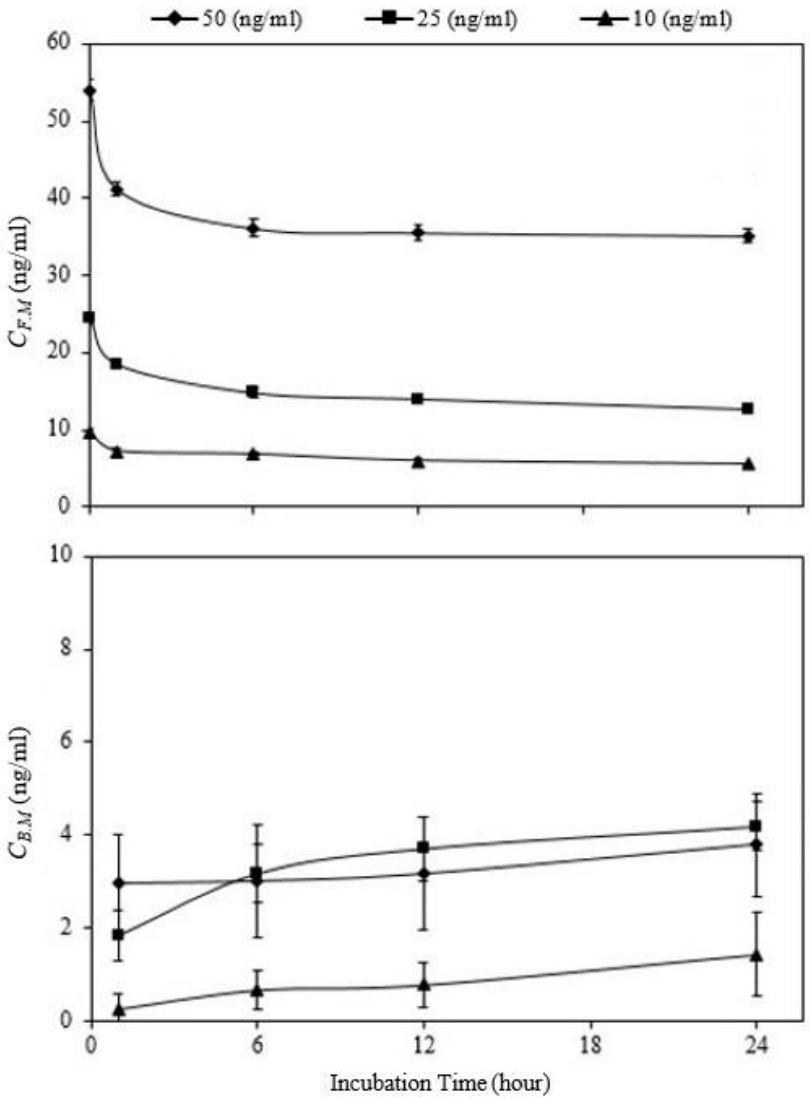

Figure 18. The concentration of free and bound MCP-1 (ng/ml) in the system for three different initial MCP-1 concentrations (10, 25, and 50 ng/ml) at the end of each incubation time. Collagen matrices were pretreated with 10, 25, and 50 ng/ml MCP-1 and incubated for 1, 6, 12, and 24 h. The concentration of free MCP-1 in the top solution was measured by ELISA and the mass balance equation was used to determine the remaining total MCP-1 concentration in the collagen matrices (as described in Materials and Methods). Values are presented as mean ± SD; n=3.

It is also shown that incubating samples for different time periods does not have a significant effect on the concentration of bound MCP-1 in the system and that the concentration is similar to the case where 25 ng/ml MCP-1 was used initially. Taken together, these results clearly show that the collagen MCP-1 binding sites in the collagen matrices is saturated using the initial MCP-1 concentration of 25-50 ng/ml.

3.6.2 Determining the order of the reaction and the reaction rate constant for MCP-1 and collagen binding

The reaction rate constant and order of the reaction was determined experimentally by measuring the initial rate of reaction for various initial MCP-1 concentrations applied to the collagen matrix, as shown in Fig. 19. The slope and intercept of the line shown in Fig. 19 are the order of the reaction (α) and natural logarithm of reaction rate constant ($\ln K_b$), respectively.

$$-\frac{dC_{F.M}}{dt} = K_b C_{F.M}^{\alpha} \qquad \text{Eq. 13}$$

$$\ln\left(-\frac{dC_{F.M}}{dt}\right) = \ln K_b + \alpha \ln C_{F.M} \qquad \text{Eq. 14}$$

$\alpha = 0.98 \approx 1$, $K_b = 0.26$ hr^{-1}

3.6.3 MCP-1 kinetics from HAEC in the 3D tissue model in the growth phase and in response to TNF-α

The kinetic profile of MCP-1 release from the 3D tissue model was determined by measuring the total concentration of MCP-1 released during the growth phase and over a 24 h time period activation with adding 10 ng/ml TNF-α. As shown in Fig. 20, total MCP-1 production from the HAEC increases significantly as the incubation time increases. The release follows a

linear trend and is used to determine the production rate of MCP-1 during the growth and activation phases (Table 2).

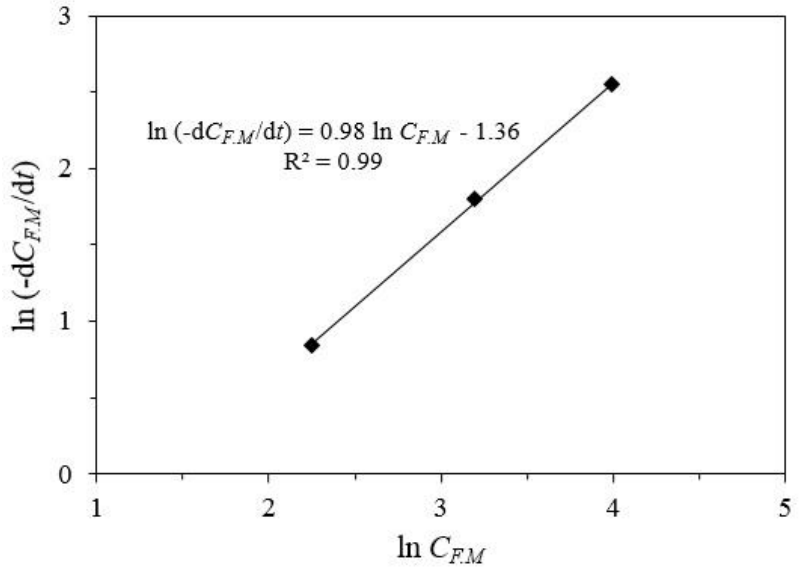

Figure 19. Initial binding reaction rate of free MCP-1 as a function of free MCP-1 concentration in the system. Three different MCP-1 concentrations (10, 25, and 50 ng/ml) were added on the cell-free collagen matrices and incubated for 1, 6, 12, and 24 h. The concentration of free MCP-1 in the top solution was measured by ELISA and the total free MCP-1 concentration in the system was determined for different MCP-1 initial concentrations and different incubation time points. Reaction rate was calculated for each initial concentrations and plotted as a function of free MCP-1 concentration that was added initially to obtain the order of the reaction and reaction rate constant experimentally. Values are presented as mean; n=3.

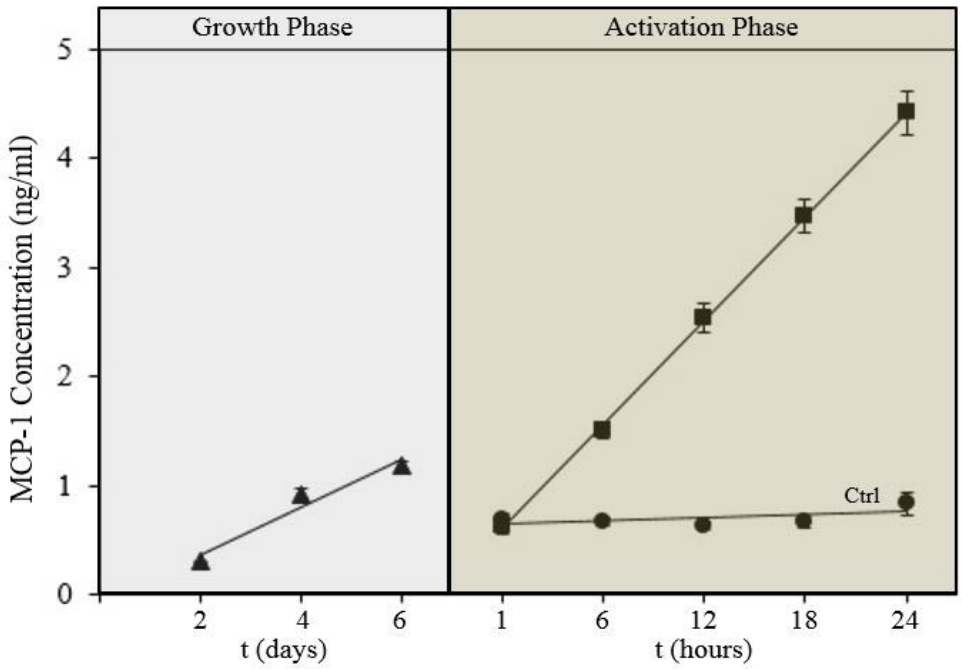

Figure 20. The total concentration of MCP-1 (ng/ml) released from HAEC in the system for the growth and activation phases. HAEC were seeded on the collagen matrix and the concentration of MCP-1 in the samples were measured by ELISA every 2 days by the end of 6 day when the cells were confluent (growth phase). Then, HAEC were treated with 10 ng/ml TNF-α and sample were incubated for 1, 6, 12, 18 and 24 h at standard conditions to measure the MCP-1 release at each activation time point. The ctrl line demonstrated the total MCP-1 released for the control samples incubated with complete media without TNF-α. Values are presented as mean ± SD; n=3.

3.7 Numerical results

3.7.1 MCP-1 concentration gradients in the 3D tissue model at the end of HAEC growth phase

As it was shown in Fig. 18, there is no bound MCP-1 in the concentrations as low as the measured MCP-1 concentration in the collagen matrices in the growth phase during 6 days post seeding HAEC on top of the collagen matrices. Therefore, the unsteady-state one dimensional mathematical model of continuity equation was solved for the free MCP-1 in the collagen matrix

with the corresponding initial and boundary conditions. Free MCP-1 concentration profile is shown in Fig. 21 as a function of distance from top surface of the collagen matrix.

Table 2. HAEC production rate of MCP-1 mass concentration during the growth and activation phases.

	MCP-1 Production Rate (ng/ml·hr)
Growth Phase ($R_{p,g}$)	0.01 ± 0.00
Activation Phase ($R_{p,a}$)	0.16 ± 0.01

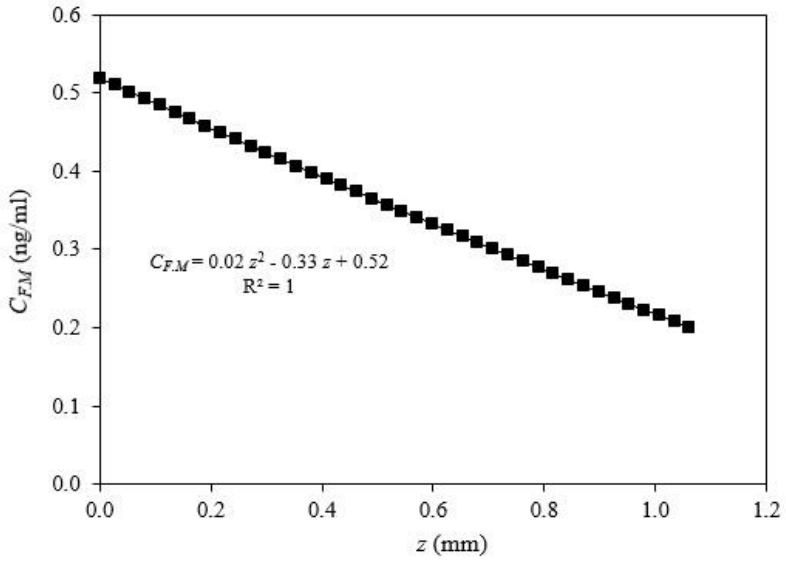

Figure 21. Concentration profile of free MCP-1 ($C_{F,M}$) in the collagen matrix of the 3D tissue model at 6 days post seeding HAEC on top of the collagen matrix in the end of growth phase, predicted by the mathematical model.

It is shown that the highest concentration of free MCP-1 is at $z = 0$ where there is a production source of MCP-1 at endothelium. The free concentration is decreasing gradually up to the bottom surface of the collagen matrix where there is a microporous membrane separating the collagen matrix from the bottom chamber.

3.7.2 MCP-1 concentration gradients within the 3D tissue model during the activation phase

A second-generation mathematical model that describes MCP-1 transport within the 3D tissue model includes a source term of MCP-1 production from the HAECs in response to TNF-α and the binding reaction of MCP-1 to the collagen matrix. The updated mathematical model equations used to describe the transport of the free and bound form of MCP-1 in the collagen matrix were solved with the two new terms of R_s and K_b, described from the previous sections. The concentration profiles of free and bound MCP-1 in the collagen matrix, as determined by the mathematical model, are shown in Fig. 22.

The developed mathematical model gives a better prediction of the concentration profiles within the vascular tissue model containing the HAEC. The model predicts the increase of MCP-1 concentration (both free and bound) with time, due to the release of MCP-1 from the HAEC in response to TNF-α activation. The second-generation model with the experimentally determined binding rate kinetics shows lower concentrations of bound MCP-1 in the system, compared to previous predictions [98]. However, the concentration of bound MCP-1 remains higher than that of the free MCP-1 after 12 h and overcomes the gradient of free MCP-1 as the time passes. This finding further substantiates that, apart from the gradient of free MCP-1, the gradient of bound MCP-1 is another potent factor that may mediate monocyte transendothelial migration.

3.8 Empirical results

MATLAB software curve fitting tool was used to fit the obtained numerical data for the 1, 6, 12, and 18 h to a 3D plane presenting the free and bound MCP-1 concentration as a function of location in the matrix and the incubation time. Polynomial curve with order of 3 and 2 in respect to *z* and *t* was selected and the empirical equation and plot for free and bound MCP-1 concentrations were obtained. The free and bound MCP-1 concentration as a function of location

and incubation time are demonstrated in Fig. 23. The relation between each concentrations, location and time is represented in Eq. 15 with the constants listed in Table 3.

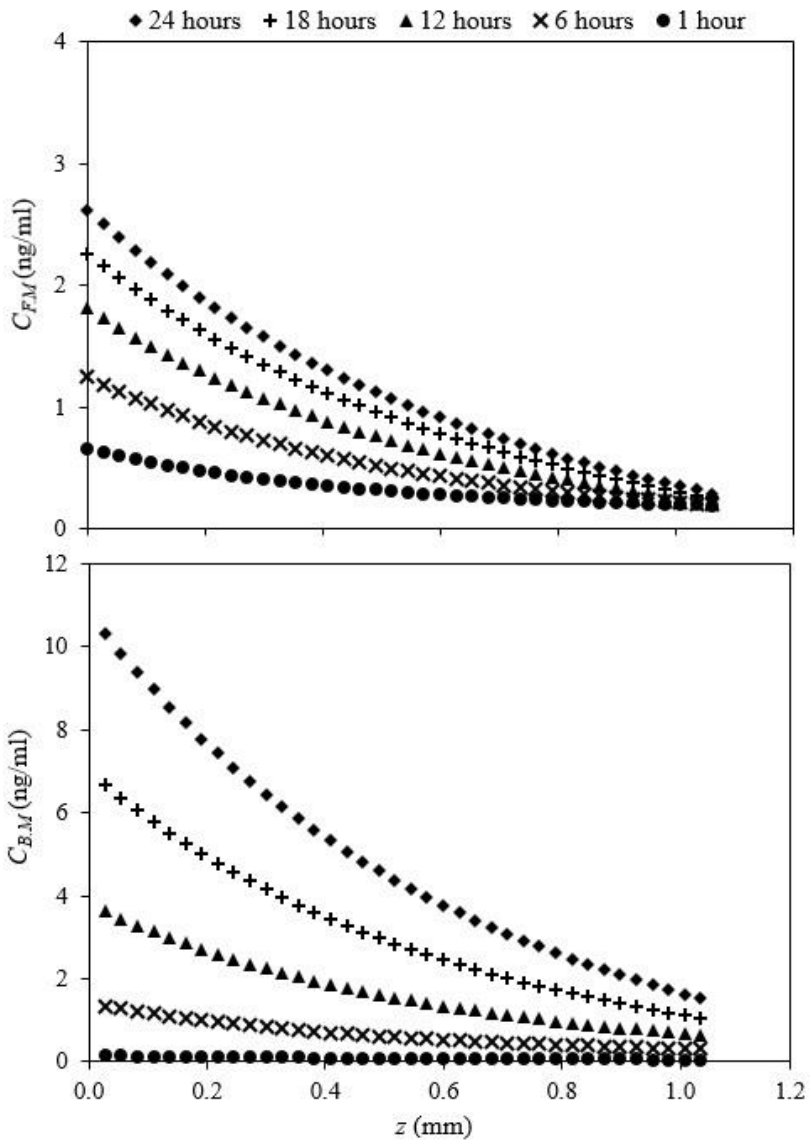

Figure 22. Concentration profiles of free ($C_{F.M}$) and bound ($C_{B.M}$) MCP-1 in the collagen matrix of the 3D tissue model, predicted by the mathematical model containing a source term to describe MCP-1 production from the HAEC and a binding reaction term to describe the interaction of MCP-1 with the collagen matrix.

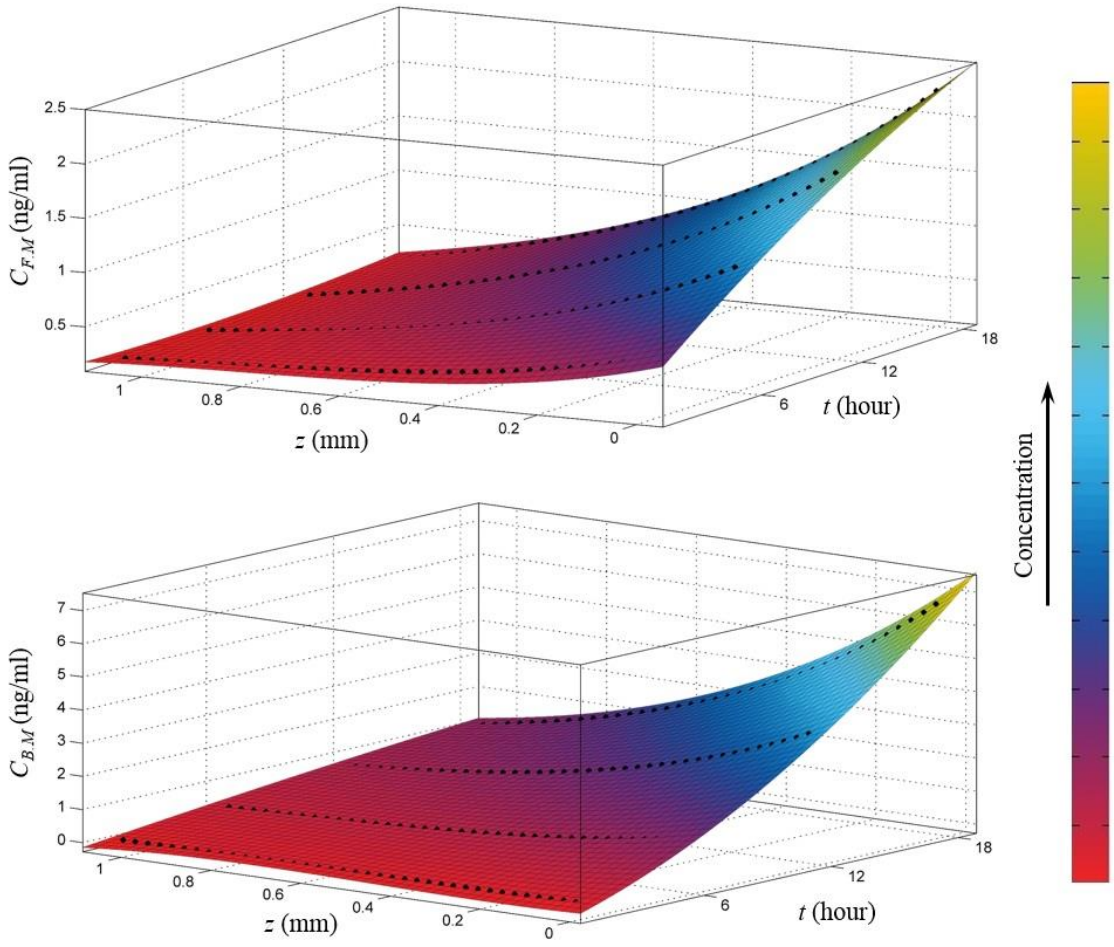

Figure 23. Concentration profiles of free ($C_{F.M}$) and bound ($C_{B.M}$) MCP-1 at each time point and location in the collagen matrix of the 3D tissue model, predicted with MATLAB curve fitting tool.

$$C_M = a + bt + cz + dt^2 + etz + fz^2 + gt^2z + htz^2 + iz^3 \quad R^2 = 0.99 \qquad \text{Eq. 15}$$

Table 3. Constants obtained from fitting the numerical data to the polynomial plane curve.

	$C_{F.M}$	$C_{B.M}$
a	0.56	-0.02
b	0.12	0.19
c	-1.15	-0.39
d	0.00	0.01
e	-0.17	-0.37
f	1.36	1.55
g	0.00	-0.01
h	0.05	0.25
i	-0.57	-1.21

Numerical results for the selected time points (1, 6, 12, and 18 h) was used for curve fitting purposes. Free and bound MCP-1 concentrations obtained for 24 h incubation time point was used as a validation for Eq. 15 with the constants listed in Table 3. Therefore, two separate locations in the collagen matrix was selected and the concentrations of free and bound MCP-1 was calculated at the selected positions at 24 h incubation time point using Eq. 15 and Table 3 constants. Obtained data are listed in Table 4 along with the numerical values and the absolute-average-percentage deviation (%AAD) of the numerical and empirical values are reported.

Table 4. Comparison between the numerical and empirical free and bound MCP-1 concentration at two different locations in the matrix after 24 h stimulation.

		Numerical		Empirical		% ADD	
t (hour)	z (mm)	$C_{F.M}$ (ng/ml)	$C_{B.M}$ (ng/ml)	$C_{F.M}$ (ng/ml)	$C_{B.M}$ (ng/ml)	$C_{F.M}$ (ng/ml)	$C_{B.M}$ (ng/ml)
24	0.136	2.09	8.55	2.09	8.72	0.00	1.99
24	0.245	1.73	7.08	1.73	7.34	0.00	3.67

Moreover, the concentration equation was integrated over the total location range in the matrix (δ) and the incubation time point to calculate the expected total MCP-1 in the collagen

matrix at each time point. The results and a comparison between the experimental and empirical results are shown in Table 5.

Table 5. Comparison between total MCP-1 in the collagen matrix at two different time points obtained from experiments and the empirical equations (Eq. 15).

	Total MCP-1 in the Collagen Matrix (ng)		
t (hours)	Experimental	Empirical	% ADD
18	1.47 ± 0.13	1.67	13.61
12	1.20 ± 0.14	0.90	25.00

3.9 Discussion

Acute and chronic inflammation responses direct the recruitment of leukocytes into the affected tissue. After adhesion of these immune cells on top of the activated endothelium, they are directed to the site of injury by chemokine concentration gradient. Specific chemokine profiles dictate migration of different leukocytes at the site of inflamed tissue. Expressed chemokines such as MCP-1 diffuses into the extracellular matrix (ECM) where they can bind to the ECM proteins and maintain, so ECM proteins are important factors for immobilizing chemokines and preserving the profile [40]. This concentration profile coordinates the cell migration and trafficking at the site of inflammation. However, the nature of these profiles has been difficult to determine *in vivo* systems.

A 3D *in vitro* vascular tissue model, consisting of human aortic endothelial cells (HAEC) grown on the surface of a collagen matrix, was developed in this study to investigate MCP-1 release within a 3D environment. The 3D tissue model provides the added dimension that is required for the creation of concentration gradients, along with cellular movement and interactions created by such gradients.

During analysis of the system, a binding reaction between MCP-1 and the collagen matrix was discovered, which shows that in addition to a gradient of free MCP-1, a bound gradient may be formed in the collagen matrix as well.

The main objective of this study was to develop a mathematical model that can be used to predict the MCP-1 concentration gradients in the collagen matrix of a 3D tissue model. The unsteady-state transport model includes a source term to describe MCP-1 production from the HAEC and a binding reaction term to describe the interaction of MCP-1 with the collagen matrix. The release of MCP-1 from the HAEC in the tissue model, under normal culture conditions and in response to TNF-α, was determined at various time points over a 24 h period. The MCP-1 release profile was used to derive the source term of MCP-1 production of the HAEC in the mathematical model.

The binding reaction expression and rate constant were determined experimentally by measuring the initial rates of reaction for various MCP-1 concentrations applied to a collagen matrix without cells. The initial concentrations of MCP-1 included in this study for determining the order of the reaction and the reaction rate constant were 10, 25, and 50 nanogram per milliliter that were physiologically relevant, and were selected based on *in vivo* and *in vitro* experiments that measured the release of MCP-1 from cells [99, 101-109] and the use of MCP-1 to direct cell migration [103, 110-114].

The mathematical model indicates that the concentration gradients of both free and bound MCP-1 are formed inside the collagen matrix. The model predicts the increase of MCP-1 concentration (both free and bound) with time, due to the release of MCP-1 from the HAECs in response to TNF-α activation. The concentration of bound MCP-1 remains higher than that of the free MCP-1 after 12 h and overcomes the gradient of free MCP-1 as time passes.

The model further substantiates that apart from the gradient of free MCP-1, the gradient of bound MCP-1 is another potent factor that may mediate monocyte transendothelial migration. The mathematical model can be used to provide new information about the relationship between MCP-1 concentration gradients and monocyte transendothelial migration associated with inflammation.

CHAPTER 5

Conclusions and Future Work

In this study, an advanced three-dimensional (3D) *in vitro* vascular tissue model was introduced as a novel tool to study the mechanisms occurring within the subendothelial extracellular matrix (ECM) during atherosclerosis. The 3D tissue model was utilized in this project to characterize cellular adhesion molecules (CAMs) and chemotactic cytokines (chemokines) that are critical participants in the transmigration of monocytes during the formation of the atherosclerotic lesion. These proteins can be potent therapeutic targets for the treatment and prevention of the inflammatory process associated with diseases like atherosclerosis. Monocyte chemoattractant protein-1 (MCP-1) is a chemokine that plays a major role in monocytes trafficking across the endothelial layer, and MCP-1 concentration gradients in the ECM are crucial in directing monocytes to the site of inflammation [53, 54, 63, 66].

The 3D tissue model consists of a collagen matrix to mimic the ECM, which provides the added dimension for the creation of a diffusive concentration gradient responsible for the control of many cellular mechanisms. In this study, human aortic endothelial cells (HAEC) were grown on the surface of the collagen matrix to investigate MCP-1 release from HAEC layer and subsequent diffusion into the ECM.

The main objective of this study was to determine the effect of MCP-1 local concentration on monocytes migration in the 3D tissue model and compare the outcomes to the traditional two-dimensional (2D) cell culture model results. We hypothesized that the MCP-1 concentration gradient within the ECM of the 3D tissue model drives a different cellular response than that in the 2D model.

This project was divided into three parts. The first part was to develop the 3D tissue model and to test the effect of the collagen matrix on endothelial cell behavior, by examining cell viability, permeability, CAMs/MCP-1 expression, and MCP-1 release under quiescent condition and when and when models were immunologically activated with tumor necrosis factor-α (TNF-α). The second objective was to compare monocyte adhesion and transmigration across the endothelial layer between the 2D and 3D models, in order to study the effect of local concentration gradients on the monocytes migration process. The third part was to develop a mathematical model to characterize the MCP-1 concentration gradients in the collagen matrix of the 3D tissue model. The amount of MCP-1 released from the endothelial cells was used to derive a mathematical model to estimate the MCP-1 concentration within the 3D tissue model at various time points and locations within the matrix.

Conclusions are summarized as follows:

i. HAEC showed high cell viability in the novel 3D tissue models. Cell viability was not significantly different than HAEC grown in the 2D models, suggesting that existence of the collagen matrix beneath the endothelium did not change cells metabolic activity.
ii. Growing HAEC on a collagen matrix altered formation of cell-cell junctions and HAEC spreading behavior according to HAEC surface area distribution analysis, which led to having a significant decrease in trans-endothelium electrical resistance of HAEC in the 3D tissue models compared to the 2D models.

iii. HAEC in both models could be activated by an inflammatory stimuli. HAEC showed an increase in the level of VCAM-1 and ICAM-1 surface expression, when activated by TNF-α.

iv. HAEC on the 2D models had significantly higher intensity of VCAM-1 and ICAM-1 expression on the surface associated with monocytes migration than the HAEC from the 3D tissue models after 24 h stimulation.

v. HAEC showed high expression of PECAM-1 in both models before and after activation which indicates that TNF-α did not have a significant effect on the PECAM-1 expression of cell-cell boundaries.

vi. MCP-1 expression on HAEC surface was upregulated with TNF-α activation at 6 h when it reached a plateau after that and remained unchanged up to 24 h stimulation for both models. HAEC had a similar MCP-1 expression time course in the 3D tissue models compared to the 2D models.

vii. Activation of the HAEC resulted in an increase in MCP-1 production. The release of MCP-1 from the HAEC in the tissue models under normal and activated culture conditions was determined at various time points over a 24 h period. The MCP-1 release profile was used to derive the source term of MCP-1 production of the HAEC in the mathematical model.

viii. MCP-1 concentration released from HAEC to the endothelium basal compartment after 24 h stimulation is shown to be identical in the 2D and 3D models. However, in fact a significant difference in the net release of MCP-1 compared to the control was observed between the collagen matrix of the 3D tissue models and the HAEC basal layer in the 2D models. Accordingly, due to the sample concentrated in the collagen matrix, resulting in an abrogated release into the surrounding media, an earlier detection of MCP-1 release was expected from the 3D tissue models. As it was shown that there was no significant difference in the MCP-1 concentration released to the basal layer of HAEC in the 2D

models after 6 h activation compared to the control samples. However, stimulating the HAEC in the 3D tissue model for 6 h had a significant effect on MCP-1 release in the collagen matrix beneath the HAEC layer.

ix. The formation of a haptotactic gradient drives an increase in the number of monocytes that migrate across the endothelial cell layer. Haptotactic gradients were only formed in the 3D tissue models and not the 2D models. There was a significant increase in the number of monocytes that migrated across the endothelial cell layer in the 3D tissue models compared to the 2D models.

x. The rate expression for the binding reaction of MCP-1 to collagen was determined experimentally by measuring the initial rates of reaction for various MCP-1 concentrations applied to a collagen matrix without cells.

xi. An unsteady-state, one-dimensional transport equation used to describe MCP-1 transport in the 3D tissue model was solved in MS-Excel with VBA using the Crank-Nicolson numerical method.

xii. The concentration gradient of MCP-1 (both free and bound) varied with position within the collagen matrix and increased over time in response to TNF-α activation. The concentration of bound MCP-1 surpasses the gradient of free MCP-1 after 12 h.

xiii. The mathematical model was validated with the measured experimental data. The numerical results obtained from solving the differential mathematical equations were fed in MATLAB software and a curve fitting tool was applied to the data to determine the best curve fit for MCP-1 concentrations at different location within the collagen matrix and different stimulation time point. Obtained equation of MCP-1 concentration as a function of location and time was used to calculate the expected total MCP-1 mass in the collagen matrix at each time point. The mathematical model demonstrated a good prediction of total MCP-1 amount within the collagen matrix for the selected incubation time points with TNF-α.

In conclusion, we have shown that kinetics and the level of CAMs expression on the cells surface and MCP-1 release in the 3D tissue model is different from the 2D model which had an effect on monocytes adhesion and transmigration through the endothelial layer between the two models. However, there is no significant difference in MCP-1 expression between two models. This 3D tissue model consisting of a collagen matrix would be a better alternative experimental model to mimic the subendothelial ECM. The added dimension is crucial for the creation of diffusive concentration gradients, which is an important factor in many physiological conditions. The concentration gradient formed in the 3D tissue model is distinctly different compared to the one in the 2D model, where the secreted factors from the endothelial cells dissolve quickly into the surrounding media. Many questions still remain about the mechanisms controlling monocytes transmigration from the blood flow to the infected tissue. With the completion of ongoing future phases, an advanced *in vitro* tissue model will be developed and can be used to study monocytes migration associated with diseases like atherosclerosis.

Consequently, future work will be directed towards addressing the following points:

1) **Describe the mechanisms involved in MCP-1 and collagen binding.** There is a large body of evidence that chemokines can bind with endothelial cell surface and ECM proteins, where the chemokines can be localized and immobilized, forming bound gradients. The binding is believed to be mediated by macromolecule polymers called glycosaminoglycans (GAGs) [44, 47, 69-75, 115]. GAGs on the cell surface and in the ECM can interact with chemokines [44, 47, 69, 70, 72, 75-81] and prevent chemokines from diffusing and being washed away by the blood shear flow [47, 74, 75, 82, 83]. The localized chemokine gradient can direct leukocytes from the blood flow to the subendothelial layer [72]. Several studies have investigated chemokine-GAG interactions in the ECM *in vivo* [71-74, 79, 83], but these interactions could not be assessed in an *in vitro* chemotaxis assay [72, 83, 87] due to the lack of the ECM to form the haptotactic

concentration gradient. GAGs can also interact with type I collagen [84, 85]; therefore, the binding reaction between MCP-1 and the collagen in this study can be mediated by GAGs, which are available from FCS in the cell growth media supplements [116]. Determining the role of GAGs in the proposed collagen/MCP-1 binding reaction will lead towards a better understanding of the underlying mechanisms in monocytes migration and atherosclerosis formation.

2) **Add fluid flow to the current models.** In the current work, the systems were all at static conditions. Static systems were used in order to simplify the development of the experimental and mathematical models used to describe MCP-1 transport and monocytes migration. Static systems can also be used to study atherosclerosis, since lesions develop predominantly at sites exposed to low or disturbed blood flow, such as branches, bends, and bifurcations in the arterial tree. Proposed theories of atherosclerosis, such as the mass transport theory and the sheer stress theory, describe altered transport of bioactive substances and cells within areas of flow stagnation with low shear stress on the endothelium. Such conditions can be represented in a static experimental system. However, an even better representation of *in vivo* conditions would be experimental and mathematical models that take the complex flow patterns into consideration. As the tools become available to create and analyze such complex models, the result may be an even better insight into the mechanisms driving monocytes migration in the early stages of atherosclerosis.

3) **Monocyte differentiation in the ECM.** Atherosclerosis is initiated by endothelial dysfunction, inflammation, and extracellular matrix (ECM) remodeling [5, 6]. Plaque formation begins with a subendothelial accumulation of lipid substances, followed by the adhesion of monocytes and lymphocytes to endothelial cells and their subsequent migration across the endothelial layer to the ECM. Monocytes differentiate into macrophages and foam cells by consuming lipid substances and interacting with low

density lipoprotein (LDL) [7-13]. The foam cells produce and release inflammatory signals that cause recruitment of additional monocytes to the area, and the development of an atherosclerosis lesion [13]. The 3D tissue model introduced in this study can be utilized to investigate the differentiation of the monocytes that migrated to the subendothelial ECM into foam cells by including additional bioactive substances involved in atherosclerosis, such as LDL. The 3D tissue model would provide a way to study the transport and accumulation of LDL in the ECM and investigate the effect of LDL transport on monocyte differentiation.

References

1. *Heart diesease and stroke prevention: addressing the national's leading killers, centers for disease control and prevention*. 2010, National centre for chronic disease prevention and health promotion: Altanta, GA.
2. Scarborough, P., et al., *Coronary heart disease statistics 2010 edition*, in *London: British Heart Foundation*. 2010.
3. Kochanek, K.D., et al., *Mortality in the United States, 2013*. 2014, Centers for disease control and prevention, national vital statistics system.
4. Epstein, F.H. and R. Ross, *Atherosclerosis—an inflammatory disease.* New England Journal of Medicine, 1999. **340**(2): p. 115-126.
5. Lusis, A.J., *Atherosclerosis.* Nature, 2000. **407**(6801): p. 233-241.
6. Newby, A.C., *An overview of the vascular response to injury: a tribute to the late Russell Ross.* Toxicology Letters, 2000. **112**: p. 519-529.
7. Harris, H., *Role of Chemotaxis in Inflammation.* Physiological Reviews, 1954. **34**(3): p. 529-562.
8. Ross, R., *The pathogenesis of atherosclerosis: a perspective for the 1990s.* Nature, 1993. **362**(6423): p. 801-809.
9. Napoli, C., et al., *Fatty streak formation occurs in human fetal aortas and is greatly enhanced by maternal hypercholesterolemia. Intimal accumulation of low density lipoprotein and its oxidation precede monocyte recruitment into early atherosclerotic lesions.* Journal of Clinical Investigation, 1997. **100**(11): p. 2680.
10. Epstein, F.H. and A.D. Luster, *Chemokines—chemotactic cytokines that mediate inflammation.* New England Journal of Medicine, 1998. **338**(7): p. 436-445.
11. Glass, C.K. and J.L. Witztum, *Atherosclerosis: the road ahead.* Cell, 2001. **104**(4): p. 503-516.
12. Bobryshev, Y.V., *Monocyte recruitment and foam cell formation in atherosclerosis.* Micron, 2006. **37**(3): p. 208-222.
13. Ley, K., et al., *Getting to the site of inflammation: the leukocyte adhesion cascade updated.* Nature Reviews Immunology, 2007. **7**(9): p. 678-689.
14. Libby, P., *Inflammation in atherosclerosis.* Nature, 2002. **420**(6917): p. 868-874.
15. Blankenberg, S., S. Barbaux, and L. Tiret, *Adhesion molecules and atherosclerosis.* Atherosclerosis, 2003. **170**(2): p. 191-203.
16. Hansson, G.K., A.L. Robertson, and C. Söderberg-Nauclér, *Inflammation and atherosclerosis.* Annual Review of Pathology: Mechanisms of Disease, 2006. **1**(1): p. 297-329.
17. Sánchez-Madrid, F. and M. Angel del Pozo, *Leukocyte polarization in cell migration and immune interactions.* The EMBO journal, 1999. **18**(3): p. 501-511.

18. Imhof, B.A. and M. Aurrand-Lions, *Adhesion mechanisms regulating the migration of monocytes.* Nature Reviews Immunology, 2004. **4**(6): p. 432-444.
19. Collins, T., *Adhesion molecules in leukocyte emigration.* Scientific American Science and Medicine, 1995. **2**: p. 28-37.
20. Koenen, R.R. and C. Weber, *Therapeutic targeting of chemokine interactions in atherosclerosis.* Nature Reviews Drug Discovery, 2010. **9**(2): p. 141-153.
21. Cybulsky, M. and M. Gimbrone, *Endothelial expression of a mononuclear leukocyte adhesion molecule during atherogenesis.* Science, 1991. **251**(4995): p. 788-791.
22. Nakashima, Y., et al., *Upregulation of VCAM-1 and ICAM-1 at atherosclerosis-prone sites on the endothelium in the ApoE-deficient mouse.* Arteriosclerosis, Thrombosis, and Vascular Biology, 1998. **18**(5): p. 842-851.
23. Van der Wal, A., et al., *Adhesion molecules on the endothelium and mononuclear cells in human atherosclerotic lesions.* The American Journal of Pathology, 1992. **141**(6): p. 1427.
24. Lawson, C. and S. Wolf, *ICAM-1 signaling in endothelial cells.* Pharmacological Reports, 2009. **61**(1): p. 22-32.
25. Wolf, S.I. and C. Lawson, *ICAM-1: Contribution to vascular inflammation and early atherosclerosis*, in *Coronary Artery DiseaseI–New Insights and Novel Approaches*, A. Squeri, Editor. 2012, InTech, Chapters published p. 65.
26. Oyu, P., M. Peclo, and A. Gown, *Various cell types in human atherosclerotic lesions express ICAM-1. Further immunocytochemical and immunochemical studies employing monoclonal antibody 10F3.* The American Journal of Pathology, 1992. **140**(4): p. 889.
27. Poston, R., et al., *Expression of intercellular adhesion molecule-1 in atherosclerotic plaques.* The American Journal of Pathology, 1992. **140**(3): p. 665.
28. Davis, C.A., et al., *Increased ICAM-l expression in aortic disease.* Journal of Vascular Surgery, 1993. **18**(5): p. 875-880.
29. Fan, J., et al., *MCP-1, ICAM-1 and VCAM-1 are present in early aneurysmal dilatation in experimental rats.* Folia Histochemica et Cytobiologica, 2010. **48**(3): p. 455-454.
30. Berman, M.E., Y. Xie, and W.A. Muller, *Roles of platelet/endothelial cell adhesion molecule-1 (PECAM-1, CD31) in natural killer cell transendothelial migration and beta 2 integrin activation.* The Journal of Immunology, 1996. **156**(4): p. 1515-1524.
31. Muller, W.A., *Leukocyte–endothelial-cell interactions in leukocyte transmigration and the inflammatory response.* Trends in Immunology, 2003. **24**(6): p. 326-333.
32. Muller, W.A., et al., *PECAM-1 is required for transendothelial migration of leukocytes.* The Journal of Experimental Medicine, 1993. **178**(2): p. 449-460.
33. DeLisser, H.M., P.J. Newman, and S.M. Albelda, *Molecular and functional aspects of PECAM-1/CD31.* Immunology Today, 1994. **15**(10): p. 490-495.
34. Nourshargh, S., F. Krombach, and E. Dejana, *The role of JAM-A and PECAM-1 in modulating leukocyte infiltration in inflamed and ischemic tissues.* Journal of Leukocyte Biology, 2006. **80**(4): p. 714-718.
35. Sawa, Y., et al., *Effects of TNF-α on Leukocyte Adhesion Molecule Expressions in Cultured Human Lymphatic Endothelium.* Journal of Histochemistry & Cytochemistry, 2007. **55**(7): p. 721-733.
36. Furie, M.B. and G.J. Randolph, *Chemokines and tissue injury.* The American Journal of Pathology, 1995. **146**(6): p. 1287.
37. Baggiolini, M., *Chemokines and leukocyte traffic.* Nature, 1998. **392**(6676): p. 565-568.
38. Reape, T.J. and P.H. Groot, *Chemokines and atherosclerosis.* Atherosclerosis, 1999. **147**(2): p. 213-225.

39. Gerard, C. and B.J. Rollins, *Chemokines and disease.* Nature Immunology, 2001. **2**(2): p. 108-115.
40. Serhan, C.N., P.A. Ward, and D.W. Gilroy, *Fundamentals of inflammation*. 2010, Cambridge University Press: Cambridge; New York. p. 175 - 185.
41. Pawlowski, N.A., et al., *The selective binding and transmigration of monocytes through the junctional complexes of human endothelium.* The Journal of Experimental Medicine, 1988. **168**(5): p. 1865-1882.
42. Huber, A.R., et al., *Regulation of transendothelial neutrophil migration by endogenous interleukin-8.* Science, 1991. **254**(5028): p. 99-102.
43. Rot, A., *Neutrophil attractant/activation protein-1 (interleukin-8) induces in vitro neutrophil migration by haptotactic mechanism.* European Journal of Immunology, 1993. **23**(1): p. 303-306.
44. Gilat, D., et al., *Regulation of adhesion of CD4+ T lymphocytes to intact or heparinase-treated subendothelial extracellular matrix by diffusible or anchored RANTES and MIP-1 beta.* The Journal of Immunology, 1994. **153**(11): p. 4899-4906.
45. Moghe, P.V., R.D. Nelson, and R.T. Tranquillo, *Cytokine-stimulated chemotaxis of human neutrophils in a 3-D conjoined fibrin gel assay.* Journal of Immunological Methods, 1995. **180**(2): p. 193-211.
46. Wiedermann, C., et al., *Different patterns of deactivation of chemotaxis and haptotaxis of human peripheral blood mononuclear leukocytes by soluble and surface-bound attractants.* Journal of Leukocyte Biology, 1995. **58**(4): p. 438-444.
47. Patel, D.D., et al., *Chemokines have diverse abilities to form solid phase gradients.* Clinical Immunology, 2001. **99**(1): p. 43-52.
48. Schumann, K., et al., *Immobilized chemokine fields and soluble chemokine gradients cooperatively shape migration patterns of dendritic cells.* Immunity, 2010. **32**(5): p. 703-713.
49. Zhao, X., et al., *Directed cell migration via chemoattractants released from degradable microspheres.* Biomaterials, 2005. **26**(24): p. 5048-5063.
50. Zigmond, S.H., *Ability of polymorphonuclear leukocytes to orient in gradients of chemotactic factors.* The Journal of Cell Biology, 1977. **75**(2): p. 606-616.
51. Janetopoulos, C. and R.A. Firtel, *Directional sensing during chemotaxis.* FEBS Letters, 2008. **582**(14): p. 2075-2085.
52. Conti, P. and M. DiGioacchino. *MCP-1 and RANTES are mediators of acute and chronic inflammation*. in *Allergy and Asthma Proceedings*. 2001. OceanSide Publications, Inc.
53. Deshmane, S.L., et al., *Monocyte chemoattractant protein-1 (MCP-1): an overview.* Journal of Interferon and Cytokine Research, 2009. **29**(6): p. 313-326.
54. Melgarejo, E., et al., *Monocyte chemoattractant protein-1: a key mediator in inflammatory processes.* The International Journal of Biochemistry & Cell Biology, 2009. **41**(5): p. 998-1001.
55. Yadav, A., V. Saini, and S. Arora, *MCP-1: chemoattractant with a role beyond immunity: a review.* International Journal of Clinical Chemistry and Diagnostic Laboratory Medicine, 2010. **411**(21): p. 1570-1579.
56. Zachariae, C.O.C., C.G. Larsen, and K. Matsushima, *Monocyte chemoattractant protein 1 (MCP-1)*, in *Encyclopedia of Immunology*, J.D. Peter, Editor. 1998, Elsevier: Oxford. p. 1748-1750.
57. Nelken, N., et al., *Monocyte chemoattractant protein-1 in human atheromatous plaques.* Journal of Clinical Investigation, 1991. **88**(4): p. 1121.

58. Ylä-Herttuala, S., et al., *Expression of monocyte chemoattractant protein 1 in macrophage-rich areas of human and rabbit atherosclerotic lesions.* Proceedings of the National Academy of Sciences, 1991. **88**(12): p. 5252-5256.
59. Takeya, M., et al., *Detection of monocyte chemoattractant protein-1 in human atherosclerotic lesions by an anti-monocyte chemoattractant protein-1 monoclonal antibody.* Human Pathology, 1993. **24**(5): p. 534-539.
60. Shin, W.S., A. Szuba, and S.G. Rockson, *The role of chemokines in human cardiovascular pathology: enhanced biological insights.* Atherosclerosis, 2002. **160**(1): p. 91-102.
61. Gu, L., et al., *Absence of monocyte chemoattractant protein-1 reduces atherosclerosis in low density lipoprotein receptor–deficient mice.* Molecular Cell, 1998. **2**(2): p. 275-281.
62. Gosling, J., et al., *MCP-1 deficiency reduces susceptibility to atherosclerosis in mice that overexpress human apolipoprotein B.* Journal of Clinical Investigation, 1999. **103**(6): p. 773-778.
63. Sozzani, S., et al., *The signal transduction pathway involved in the migration induced by a monocyte chemotactic cytokine.* The Journal of Immunology, 1991. **147**(7): p. 2215-2221.
64. Takeya, M., et al., *Production of monocyte chemoattractant protein-1 by malignant fibrous histiocytoma: relation to the origin of histiocyte-like cells.* Experimental and Molecular Pathology, 1991. **54**(1): p. 61-71.
65. Zoja, C., et al., *Interleukin-1 beta and tumor necrosis factor-alpha induce gene expression and production of leukocyte chemotactic factors, colony-stimulating factors, and interleukin-6 in human mesangial cells.* The American Journal of Pathology, 1991. **138**(4): p. 991.
66. Randolph, G.J. and M.B. Furie, *A soluble gradient of endogenous monocyte chemoattractant protein-1 promotes the transendothelial migration of monocytes in vitro.* The Journal of Immunology, 1995. **155**(7): p. 3610-3618.
67. Douglas, M., et al., *Endothelial production of MCP-1: modulation by heparin and consequences for mononuclear cell activation.* Immunology, 1997. **92**(4): p. 512-518.
68. Weber, K.S., et al., *Differential immobilization and hierarchical involvement of chemokines in monocyte arrest and transmigration on inflamed endothelium in shear flow.* European Journal of Immunology, 1999. **29**(2): p. 700-712.
69. Witt, D.P. and A.D. Lander, *Differential binding of chemokines to glycosaminoglycan subpopulations.* Current Biology, 1994. **4**(5): p. 394-400.
70. Kuschert, G.S., et al., *Identification of a glycosaminoglycan binding surface on human interleukin-8.* Biochemistry, 1998. **37**(32): p. 11193-11201.
71. Frevert, C.W., et al., *Tissue-specific mechanisms control the retention of IL-8 in lungs and skin.* The Journal of Immunology, 2002. **168**(7): p. 3550-3556.
72. Johnson, Z., et al., *Chemokine inhibition-why, when, where, which and how?* Biochemical Society Transactions, 2004. **32**(2): p. 366-377.
73. Lau, E.K., et al., *Identification of the glycosaminoglycan binding site of the CC chemokine, MCP-1.* Journal of Biological Chemistry, 2004. **279**(21): p. 22294-22305.
74. Johnson, Z., A. Proudfoot, and T. Handel, *Interaction of chemokines and glycosaminoglycans: a new twist in the regulation of chemokine function with opportunities for therapeutic intervention.* Cytokine & Growth Factor Reviews, 2005. **16**(6): p. 625-636.
75. Alon, R., *Trapped versus soluble chemokines: functions in leukocyte adhesion and motility.* Immunity, 2010. **33**(5): p. 654-656.

76. Chakravarty, L., et al., *Lysine 58 and histidine 66 at the c-terminal α-Helix of monocyte chemoattractant protein-1 are essential for glycosaminoglycan binding.* Journal of Biological Chemistry, 1998. **273**(45): p. 29641-29647.
77. Koopmann, W., C. Ediriwickrema, and M.S. Krangel, *Structure and function of the glycosaminoglycan binding site of chemokine macrophage-inflammatory protein-1β.* The Journal of Immunology, 1999. **163**(4): p. 2120-2127.
78. Krieger, E., et al., *A structural and dynamic model for the interaction of interleukin-8 and glycosaminoglycans: Support from isothermal fluorescence titrations.* Proteins: Structure, Function, and Bioinformatics, 2004. **54**(4): p. 768-775.
79. Yu, Y., et al., *Chemokine-glycosaminoglycan binding: specificity for CCR2 ligand binding to highly sulfated oligosaccharides using FTICR mass spectrometry.* Journal of Biological Chemistry, 2005. **280**(37): p. 32200-32208.
80. Proudfoot, A.E., *The biological relevance of chemokine-proteoglycan interactions.* Biochemical Society Transactions, 2006. **34**(3): p. 422.
81. Allen, S.J., S.E. Crown, and T.M. Handel, *Chemokine: receptor structure, interactions, and antagonism.* Annual Review of Immunology, 2007. **25**: p. 787-820.
82. Antal, R., *Endothelial cell binding of NAP-1/IL-8: role in neutrophil emigration.* Immunology Today, 1992. **13**(8): p. 291-294.
83. Proudfoot, A.E., et al., *Glycosaminoglycan binding and oligomerization are essential for the in vivo activity of certain chemokines.* Proceedings of the National Academy of Sciences, 2003. **100**(4): p. 1885-1890.
84. Raspanti, M., et al., *Glycosaminoglycans show a specific periodic interaction with type I collagen fibrils.* Journal of Structural Biology, 2008. **164**(1): p. 134-139.
85. Lungu, A., et al., *The influence of glycosaminoglycan type on the collagen-glycosaminoglycan porous scaffolds.* Digest Journal of Nanomaterials and Biostructures, 2011. **6**(4): p. 1867-1875.
86. Distler, J.H., et al., *Monocyte chemoattractant protein 1 released from glycosaminoglycans mediates its profibrotic effects in systemic sclerosis via the release of interleukin-4 from T cells.* Arthritis and Rheumatism, 2006. **54**(1): p. 214-225.
87. Kuschert, G.S., et al., *Glycosaminoglycans interact selectively with chemokines and modulate receptor binding and cellular responses.* Biochemistry, 1999. **38**(39): p. 12959-12968.
88. Rollins, B.J., *Monocyte chemoattractant protein 1: a potential regulator of monocyte recruitment in inflammatory disease.* Molecular Medicine Today, 1996. **2**(5): p. 198-204.
89. Wain, J., J. Kirby, and S. Ali, *Leucocyte chemotaxis: Examination of mitogen-activated protein kinase and phosphoinositide 3-kinase activation by Monocyte Chemoattractant Proteins-1,-2,-3 and -4.* Clinical & Experimental Immunology, 2002. **127**(3): p. 436-444.
90. Arefieva, T.I., et al., *MCP-1-stimulated chemotaxis of monocytic and endothelial cells is dependent on activation of different signaling cascades.* Cytokine, 2005. **31**(6): p. 439-446.
91. Haycock, J.W., *3D cell culture methods and protocols*. 2011, New York, NY: Humana Press.
92. Hardy, L.A., et al., *Examination of MCP-1 (CCL2) partitioning and presentation during transendothelial leukocyte migration.* Laboratory Investigation, 2004. **84**(1): p. 81-90.
93. Adams, D.H. and A. Rlloyd, *Chemokines: leucocyte recruitment and activation cytokines.* The Lancet, 1997. **349**(9050): p. 490-495.
94. Devalaraja, M.N. and A. Richmond, *Multiple chemotactic factors: fine control or redundancy?* Trends in Pharmacological Sciences, 1999. **20**(4): p. 151-156.

95. Moser, B. and P. Loetscher, *Lymphocyte traffic control by chemokines.* Nature Immunology, 2001. **2**(2): p. 123-128.
96. Wang, Y. and D.J. Irvine, *Engineering chemoattractant gradients using chemokine-releasing polysaccharide microspheres.* Biomaterials, 2011. **32**(21): p. 4903-4913.
97. Gappa-Fahlenkamp, H. and A. Shukla, *The effect of short-term, high glucose concentration on endothelial cells and leukocytes in a 3D in vitro human vascular tissue model.* In Vitro Cellular & Developmental Biology-Animal, 2009. **45**(5-6): p. 234-242.
98. Leemasawatdigul, K. and H. Gappa-Fahlenkamp, *Development of a mathematical model to describe the transport of monocyte chemoattractant protein-1 through a three-dimensional collagen matrix.* Cardiovascular Pathology, 2012. **21**(3): p. 219-228.
99. Lukacs, N.W., et al., *Production of chemokines, interleukin-8 and monocyte chemoattractant protein-1, during monocyte: endothelial cell interactions.* Blood, 1995. **86**(7): p. 2767-2773.
100. Muller, W.A. and S.A. Weigl, *Monocyte-selective transendothelial migration: dissection of the binding and transmigration phases by an in vitro assay.* The Journal of Experimental Medicine, 1992. **176**(3): p. 819-828.
101. Vos, D., *Analysis of the secretion pattern of monocyte chemotactic protein-1 (MCP-1) and transforming growth factor-beta 2 (TGF-β2) by human retinal pigment epithelial cells.* Clinical and Experimental Immunology, 1999. **118**(1): p. 35-40.
102. Uriarte, S.M., et al., *Effects of fluoroquinolones on the migration of human phagocytes through Chlamydia pneumoniae-infected and tumor necrosis factor alpha-stimulated endothelial cells.* Antimicrobial Agents and Chemotherapy, 2004. **48**(7): p. 2538-2543.
103. Weber, K.S., et al., *Expression of CCR2 by endothelial cells implications for MCP-1 mediated wound injury repair and in vivo inflammatory activation of endothelium.* Arteriosclerosis, Thrombosis, and Vascular Biology, 1999. **19**(9): p. 2085-2093.
104. Addabbo, F., et al., *Globular adiponectin counteracts VCAM-1-mediated monocyte adhesion via AdipoR1/NF-κB/COX-2 signaling in human aortic endothelial cells.* American Journal of Physiology.Endocrinology and Metabolism, 2011. **301**(6): p. E1143-E1154.
105. Ju, Y., et al., *Modulation of TNF-α-induced endothelial cell activation by glucosamine, a naturally occurring amino monosaccharide.* International Journal of Molecular Medicine, 2008. **22**(6): p. 809-815.
106. Pasceri, V., et al., *Modulation of C-reactive protein–mediated monocyte chemoattractant protein-1 induction in human endothelial cells by anti-atherosclerosis drugs.* Circulation, 2001. **103**(21): p. 2531-2534.
107. Panicker, S.R., et al., *Quercetin attenuates Monocyte Chemoattractant Protein-1 gene expression in glucose primed aortic endothelial cells through NF-κB and AP-1.* Pharmacological Research, 2010. **62**(4): p. 328-336.
108. De Lemos, J.A., et al., *Association between plasma levels of monocyte chemoattractant protein-1 and long-term clinical outcomes in patients with acute coronary syndromes.* Circulation, 2003. **107**(5): p. 690-695.
109. Jilma Stohlawetz, P., et al., *Fy phenotype and gender determine plasma levels of monocyte chemotactic protein.* Transfusion, 2001. **41**(3): p. 378-381.
110. Kränkel, N., et al., *A novel flow cytometry-based assay to study leukocyte–endothelial cell interactions in vitro.* Cytometry Part A, 2011. **79**(4): p. 256-262.
111. Lührmann, A., et al., *The alveolar epithelial type I-like cell line as an adequate model for leukocyte migration studies in vitro.* Experimental and Toxicologic Pathology, 2007. **58**(5): p. 277-283.

112. Weber, C., et al., *Differential chemokine receptor expression and function in human monocyte subpopulations.* Journal of Leukocyte Biology, 2000. **67**(5): p. 699-704.
113. Weber, C., et al., *Downregulation by tumor necrosis factor-α of monocyte CCR2 expression and monocyte chemotactic protein-1-induced transendothelial migration is antagonized by oxidized low-density lipoprotein: A potential mechanism of monocyte retention in atherosclerotic lesions.* Atherosclerosis, 1999. **145**(1): p. 115-123.
114. Weber, C., et al., *Role of alpha L beta 2 integrin avidity in transendothelial chemotaxis of mononuclear cells.* The Journal of Immunology, 1997. **159**(8): p. 3968-3975.
115. Jose L. de Paz a, P.H.S., *Deciphering the glycosaminoglycan code with the help of microarrays.* Molecular Biosystems, 2008. **4**(7): p. 707-711.
116. Lu, H., et al., *Glycosaminoglycans in human and bovine serum: detection of twenty-four heparan sulfate and chondroitin sulfate motifs including a novel sialic acid-modified chondroitin sulfate linkage hexasaccharide.* Glycobiol Insights, 2010. **9**(2): p. 13-28.

VITA

NEDA GHOUSIFAM

Candidate for the Degree of

Doctor of Philosophy

Thesis: THE EFFECT OF MONOCYTE CHEMOATTRACTANT PROTEIN-1 CONCENTRATION GRADIENTS ON MONOCYTE MIGRATION IN A THREE-DIMENSIONAL *IN VITRO* VASCULAR TISSUE MODEL

Major Field: CHEMICAL ENGINEERING

Biographical:

Education:
•Completed the requirements for the Doctor of Philosophy in chemical engineering at Oklahoma State University, Stillwater, Oklahoma in July, 2015.
•Completed the requirements for the Master of Science in chemical engineering at Oklahoma State University, Stillwater, Oklahoma in May, 2015.
•Completed the requirements for the Bachelor of Science in chemical engineering at Sharif University of Technology, Tehran, Tehran/IRAN in May, 2008.

Experience:
Research Experience:
•A 3D Vascular Tissue Model for Studying Cell Migration in Atherosclerosis (NIH 1R15EB009527-0): A 3D human *in vitro* tissue model development that recapitulates the interface between a blood vessel and the surrounding tissue.
•Designing a Freeze Dryer for Pharmaceutical Processes: Pre-Feas Study for "Alborz" pharmaceutical company in Tehran, Iran (Spring 2009)
•Internship at Pasteur Institute of Iran: Synthesis of dendrimers and preparation of Au, Ag, Cu, and Zn Nanoparticles, Tehran, Iran (Summer 2008)

Mentoring Experience:
•Lane, J. (Fall 2014), W.W. Allen Scholar Research Project.
•Sanders, C. (Summer 2012), Annual Lew Wentz Foundation Research Project.
•Keenum, A. (Spring 2012), Annual Lew Wentz Foundation Research Project.
•Williams, L. (Spring 2012), Annual Lew Wentz Foundation Research Project.
•Vera, M. (Spring 2011), Annual Lew Wentz Foundation Research Project.

Teaching Experience:
•Teaching Assistant, Undergraduate Students, Oklahoma State University
"Introduction to Chemical Reaction Engineering" (Spring 2015)
"Introduction to Chemical Process Engineering" (Spring 2012)
•Tutor, Junior and Senior High School Students, Tehran, Iran
Chemistry, Physics, Mathematics, and English